

## Durham Research Online

---

### Deposited in DRO:

27 August 2020

### Version of attached file:

Published Version

### Peer-review status of attached file:

Peer-reviewed

### Citation for published item:

McClymont, E.L. and Ford, H. and Ho, S.-L. and Tindall, J. and Haywood, A.M. and Alonso-Garcia, M. and Bailey, I. and Berke, M. A. and Littler, K. and Patterson, M. and Petrick, B. and Peterse, F. and Ravelo, A. C. and Risebrobakken, B. and Schepper, S. De and Swann, G. E. A. and Thirumalai, K. and Tierney, J. E. and Weijst, C. van der and White, S. and Abe-Ouchi, A. and Baatsen, M.L.J. and Brady, E.C. and Chan, W.-L. and Chandan, D. and Feng, R. and Guo, C. and von der Heydt, A.S. and Hunter, S. and Li, X. and Lohmann, G. and Nisancioglu, K.H. and Otto-Bliesner, B.L. and Peltier, W.R. and Stepanek, C. and Zhang, Z. (2020) 'Lessons from a high CO<sub>2</sub> world : an ocean view from 3 million years ago.', *Climate of the past*, 16 (4). pp. 1599-1615.

### Further information on publisher's website:

<https://doi.org/10.5194/cp-16-1599-2020>

### Publisher's copyright statement:

© Author(s) 2020. This work is distributed under the Creative Commons Attribution 4.0 License.

### Additional information:

## Use policy

---

The full-text may be used and/or reproduced, and given to third parties in any format or medium, without prior permission or charge, for personal research or study, educational, or not-for-profit purposes provided that:

- a full bibliographic reference is made to the original source
- a [link](#) is made to the metadata record in DRO
- the full-text is not changed in any way

The full-text must not be sold in any format or medium without the formal permission of the copyright holders.

Please consult the [full DRO policy](#) for further details.



## Lessons from a high-CO<sub>2</sub> world: an ocean view from ~ 3 million years ago

Erin L. McClymont<sup>1</sup>, Heather L. Ford<sup>2</sup>, Sze Ling Ho<sup>3</sup>, Julia C. Tindall<sup>4</sup>, Alan M. Haywood<sup>4</sup>,  
Montserrat Alonso-Garcia<sup>5,6</sup>, Ian Bailey<sup>7</sup>, Melissa A. Berke<sup>8</sup>, Kate Littler<sup>7</sup>, Molly O. Patterson<sup>9</sup>, Benjamin Petrick<sup>10</sup>,  
Francien Peterse<sup>11</sup>, A. Christina Ravelo<sup>12</sup>, Bjørge Risebrobakken<sup>13</sup>, Stijn De Schepper<sup>13</sup>, George E. A. Swann<sup>14</sup>,  
Kaustubh Thirumalai<sup>15</sup>, Jessica E. Tierney<sup>15</sup>, Carolien van der Weijst<sup>11</sup>, Sarah White<sup>16</sup>, Ayako Abe-Ouchi<sup>17,18</sup>,  
Michiel L. J. Baatsen<sup>19</sup>, Esther C. Brady<sup>20</sup>, Wing-Le Chan<sup>17</sup>, Deepak Chandan<sup>21</sup>, Ran Feng<sup>22</sup>, Chuncheng Guo<sup>13</sup>,  
Anna S. von der Heydt<sup>19</sup>, Stephen Hunter<sup>4</sup>, Xiangyi Li<sup>13,23</sup>, Gerrit Lohmann<sup>24</sup>, Kerim H. Nisancioglu<sup>13,25,26</sup>,  
Bette L. Otto-Bliesner<sup>20</sup>, W. Richard Peltier<sup>21</sup>, Christian Stepanek<sup>24</sup>, and Zhongshi Zhang<sup>13,27,28</sup>

<sup>1</sup>Department of Geography, Durham University, Durham, DH1 3LE, UK

<sup>2</sup>School of Geography, Queen Mary University of London, London, E1 4NS, UK

<sup>3</sup>Institute of Oceanography, National Taiwan University, 10617 Taipei, Taiwan

<sup>4</sup>School of Earth and Environment, University of Leeds, Leeds, LS29JT, UK

<sup>5</sup>Department of Geology, University of Salamanca, Salamanca, Spain

<sup>6</sup>CCMAR, Universidade do Algarve, 8005-139 Faro, Portugal

<sup>7</sup>Camborne School of Mines & Environment and Sustainability Institute, University of Exeter, Exeter, TR10 9FE, UK

<sup>8</sup>Department of Civil and Environmental Engineering and Earth Sciences, University of Notre Dame,  
Notre Dame, IN 46656, USA

<sup>9</sup>Department of Geological Sciences and Environmental Studies, Binghamton University SUNY, 4400 Vestal Pkwy E,  
Binghamton, New York, USA

<sup>10</sup>Climate Geochemistry Department, Max Planck Institute for Chemistry, 55128 Mainz, Germany

<sup>11</sup>Department of Earth Sciences, Utrecht University, Utrecht, 3584 CB, the Netherlands

<sup>12</sup>Department of Ocean Sciences, University of California, Santa Cruz, CA 95064, USA

<sup>13</sup>NORCE Norwegian Research Centre and Bjerknes Centre for Climate Research, 5007 Bergen, Norway

<sup>14</sup>School of Geography, University of Nottingham, Nottingham, NG7 2RD, UK

<sup>15</sup>Department of Geosciences, The University of Arizona, Tucson, AZ 85721, USA

<sup>16</sup>Department of Earth and Planetary Sciences, University of California, Santa Cruz, CA 95064, USA

<sup>17</sup>Atmosphere and Ocean Research Institute, The University of Tokyo, Kashiwa, 277-8564, Japan

<sup>18</sup>National Institute for Polar Research, Tachikawa, 190-8518, Japan

<sup>19</sup>Institute for Marine and Atmospheric research Utrecht (IMAU), Department of Physics, Utrecht University,  
Utrecht, 3584 CC, the Netherlands

<sup>20</sup>Climate and Global Dynamics Laboratory, National Center for Atmospheric Research (NCAR), Boulder, CO 80305, USA

<sup>21</sup>Department of Physics, University of Toronto, Toronto, M5S 1A7, Canada

<sup>22</sup>Department of Geosciences, University of Connecticut, Storrs, CT 06033, USA

<sup>23</sup>Climate Change Research Center, Institute of Atmospheric Physics, Chinese Academy of Sciences, Beijing 100029, China

<sup>24</sup>Alfred-Wegener-Institut – Helmholtz-Zentrum für Polar und Meeresforschung (AWI), Bremerhaven, 27570, Germany

<sup>25</sup>Department of Earth Science, University of Bergen, Allégaten 70, 5007 Bergen, Norway

<sup>26</sup>Centre for Earth Evolution and Dynamics, University of Oslo, P.O. Box 1028, Blindern, 0315 Oslo, Norway

<sup>27</sup>Department of Atmospheric Science, School of Environmental Studies, China University of Geosciences, Wuhan, China

<sup>28</sup>Nansen-Zhu International Research Centre, Institute of Atmospheric Physics, Chinese Academy  
of Sciences, Beijing 100029, China

**Correspondence:** Erin L. McClymont ([erin.mcclymont@durham.ac.uk](mailto:erin.mcclymont@durham.ac.uk)), Heather L. Ford ([h.ford@qmul.ac.uk](mailto:h.ford@qmul.ac.uk)),  
and Sze Ling Ho ([slingho@ntu.edu.tw](mailto:slingho@ntu.edu.tw))

Received: 20 December 2019 – Discussion started: 9 January 2020

Revised: 19 June 2020 – Accepted: 2 July 2020 – Published: 27 August 2020

**Abstract.** A range of future climate scenarios are projected for high atmospheric CO<sub>2</sub> concentrations, given uncertainties over future human actions as well as potential environmental and climatic feedbacks. The geological record offers an opportunity to understand climate system response to a range of forcings and feedbacks which operate over multiple temporal and spatial scales. Here, we examine a single interglacial during the late Pliocene (KM5c, ca.  $3.205 \pm 0.01$  Ma) when atmospheric CO<sub>2</sub> exceeded pre-industrial concentrations, but were similar to today and to the lowest emission scenarios for this century. As orbital forcing and continental configurations were almost identical to today, we are able to focus on equilibrium climate system response to modern and near-future CO<sub>2</sub>. Using proxy data from 32 sites, we demonstrate that global mean sea-surface temperatures were warmer than pre-industrial values, by  $\sim 2.3$  °C for the combined proxy data (foraminifera Mg/Ca and alkenones), or by  $\sim 3.2$ – $3.4$  °C (alkenones only). Compared to the pre-industrial period, reduced meridional gradients and enhanced warming in the North Atlantic are consistently reconstructed. There is broad agreement between data and models at the global scale, with regional differences reflecting ocean circulation and/or proxy signals. An uneven distribution of proxy data in time and space does, however, add uncertainty to our anomaly calculations. The reconstructed global mean sea-surface temperature anomaly for KM5c is warmer than all but three of the PlioMIP2 model outputs, and the reconstructed North Atlantic data tend to align with the warmest KM5c model values. Our results demonstrate that even under low-CO<sub>2</sub> emission scenarios, surface ocean warming may be expected to exceed model projections and will be accentuated in the higher latitudes.

## 1 Introduction

By the end of this century, projected atmospheric CO<sub>2</sub> concentrations range from 430 to  $> 1000$  ppmv depending upon future emission scenarios (IPCC, 2014a). At the current rate of emissions, global mean temperatures are projected to exceed 1.5 and 2 °C above pre-industrial values in 10 and 20 years, respectively, passing the targets set by the Paris Agreement (IPCC, 2019). The geological record affords an opportunity to explore key global and regional climate responses to different atmospheric CO<sub>2</sub> concentrations, including those which extend beyond centennial timescales (Fischer et al., 2018). Palaeoclimate models indicate that climates last experienced during the mid-Piacenzian stage of the Pliocene (3.1–3.3 Ma) will be surpassed by 2030 CE under high-emission scenarios (Representative Concentration

Pathway, RCP8.5) or will develop by 2040 CE and be sustained thereafter under more moderate emissions (RCP4.5; Burke et al., 2018).

The late Pliocene thus provides a geological analogue for climate response to moderate CO<sub>2</sub> emissions. However, the magnitude of tropical ocean warming differs between proxy reconstructions (e.g. Zhang et al., 2014; O'Brien et al., 2014; Ford and Ravelo, 2019; Tierney et al., 2019a), and stronger polar amplification has been consistently recorded in proxy data compared to models (Haywood et al., 2013, 2016a). Some of the disagreements may reflect non-thermal influences on temperature proxies (e.g. secular evolution of seawater Mg/Ca; Medina-Elizalde et al., 2008; Evans et al., 2016) and/or seasonality in the recorded signals (e.g. Tierney and Tingley, 2018). It has also been proposed that previous approaches to integrating Pliocene sea-surface temperature (SST) data may have introduced bias to data–model comparison (Haywood et al., 2013). For example, the Pliocene Research Interpretation and Synoptic Mapping (PRISM) project generated warm peak averages within specified time windows (Fig. 1) (outlined in Dowsett et al., 2016, and references therein). However, by integrating multiple warm peaks within the 3.1–3.3 Ma mid-Piacenzian data synthesis windows (Fig. 1), regional and time-transgressive responses to orbital forcing (Prescott et al., 2014; Fischer et al., 2018; Hoffman et al., 2017; Feng et al., 2017) are potentially recorded in the proxy data, which may not align with the more narrowly defined time interval being modelled (Haywood et al., 2013; Dowsett et al., 2016).

Here, we present a new, globally distributed synthesis of SST data for the mid-Piacenzian stage, addressing two concerns. First, we minimise the impact of orbital forcing on regional and global climate signals by synthesising data from a specific interglacial stage: a 20 kyr time slice centred on 3.205 Ma (KM5c; see Fig. 1). At 3.205 Ma, both seasonal and regional distributions of incoming insolation are close to modern values, making this time an important analogue for 21st-century climate (Haywood et al., 2013). The low variability in orbital forcing through KM5c minimises the potential for time-transgressive regional signals to be a feature of the geological data (Haywood et al., 2013; Prescott et al., 2014). Second, we provide a range of estimates from different SST proxies, taking into consideration the uncertainties in proxy-to-temperature calibrations and/or secular processes that may bias proxy estimates. This synthesis is possible due to robust stratigraphic constraints placed on the datasets by the PAGES-PlioVAR working group (see Sect. 2.2).

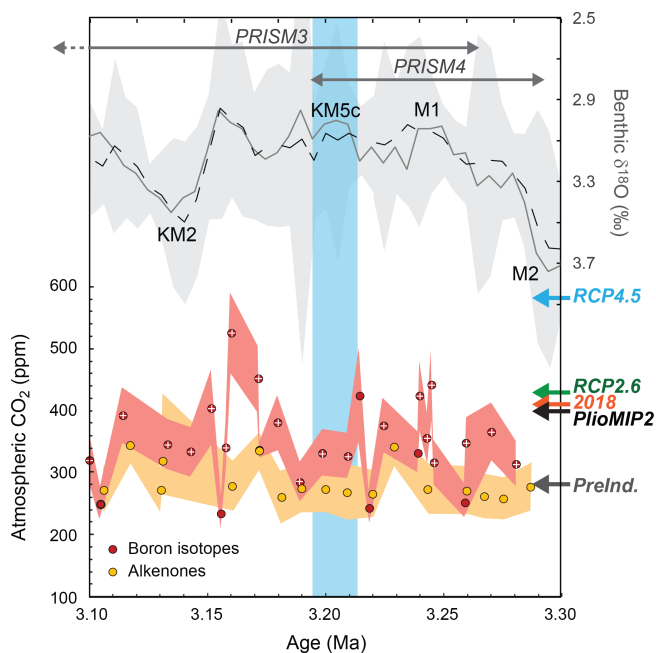


**Figure 1.** The KM5c interglacial during the late Pliocene (3.195–3.215 Ma). Upper part of graph: benthic oxygen isotope stack (solid line: LR04, Lisiecki and Raymo, 2005; dashed line and grey shading: Prob-stack mean and 95 % confidence interval, respectively, Ahn et al., 2017). Selected Marine Isotope Stages (KM2 through to M2) are highlighted. The KM5c interval of focus here is indicated by the shaded blue bar. Previous Pliocene synthesis intervals are also shown: PRISM3 (3.025–3.264 Ma) and PRISM4 (isotope stages KM5c–M2; Dowsett et al., 2016). Lower part of graph: reconstructed atmospheric CO<sub>2</sub> concentrations (Foster et al., 2017). Points show mean reported data (except white crosses: median values from Martinez-Boti et al., 2015); shading shows reported upper and lower estimates. Past and projected atmospheric CO<sub>2</sub> concentrations highlighted by arrows: PlioMIP2 simulations are run with CO<sub>2</sub> at 400 ppmv (Haywood et al., 2020) close to the annual mean in 2018 (NOAA). Pre-industrial values from ice cores (Loulerge et al., 2008) and projected representative concentration pathways (RCP) for 2100 CE (IPCC, 2013).

## 2 Methods

### 2.1 The KM5c interglacial

KM5c (also referred to as KM5.3) is an interglacial centred on a  $\sim 100$  kyr window of relatively depleted benthic  $^{18}\text{O}$  values, which immediately follows a pronounced  $\delta^{18}\text{O}$  peak during the glacial stage M2 (3.3 Ma; Fig. 1). Minor changes to orbital forcing during KM5 enables a wider target zone (3.205 Ma  $\pm$  20 kyr) for data collection because the potential for orbitally forced regional and time-transgressive climate signals is minimised (Haywood et al., 2013). A comparable approach has been adopted by the PRISM4 synthesis (3.190 to 3.220 Ma; Foley and Dowsett, 2019; see Fig. 1). Here, we focus on a narrow time slice from 3.195 to 3.215 Ma, to span approximately one precession cycle. The recon-

structed atmospheric CO<sub>2</sub> concentrations from boron isotopes in KM5c are  $360 \pm 55$  ppmv (for median boron-derived values ( $n = 3$ ), full range: 289–502 ppmv, Fig. 1; Foster et al., 2017). A wider range of atmospheric CO<sub>2</sub> concentrations has been reconstructed for the whole mid-Piacenzian stage ( $356 \pm 65$  ppmv for median values ( $n = 36$ ), full range: 185–592 ppmv; Foster et al., 2017).

### 2.2 Age models

The PAGES-PlioVAR working group agreed on a set of stratigraphic protocols to maximise confidence in the identification and analysis of orbital-scale variability within the mid-Piacenzian stage (McClymont et al., 2017). Sites were only included in the synthesis if they had either (i)  $\leq 10$  kyr resolution benthic  $\delta^{18}\text{O}$  data which could be (or had been) tied to the LR04 stack (Lisiecki and Raymo, 2005) or the HMM-Stack (Ahn et al., 2017) and/or (ii) the palaeomagnetic tie points for upper Mammoth (C2An.2n (b) at 3.22 Ma) and lower Mammoth (C2An.3n (t) at 3.33 Ma). At one site (ODP Site 1090) these conditions were not met (see Supplement), but tuning to LR04 had been made using a record of dust concentrations under the assumption that higher dust flux occurred during glacials as observed during the Pleistocene (Martinez-Garcia et al., 2011). At ODP Site 806, uncertainty over age control resulted from the absence of an agreed splice across the multiple holes drilled by ODP, and a new age model has been constructed (see Supplement). For some sites (see online summary at <https://pliovar.github.io/km5c.html>, last access: 30 June 2020), revisions to the published age model were made, for example if the original data had been published prior to the LR04 stack (Lisiecki and Raymo, 2005) or prior to revisions to the palaeomagnetic timescale (Gradstein et al., 2012). In total, data from 32 sites were compiled, extending from 46° S to 69° N (Fig. 2).

### 2.3 Proxy SST data

A multi-proxy approach was taken, to maximise the information available on changing climates and environments during the KM5c interval. Two SST proxies were analysed: the alkenone-derived  $U_{37}^{K'}$  index (Prahl and Wakeham, 1987) and foraminifera calcite Mg/Ca (Delaney et al., 1985). Both proxies have several calibrations to modern SST: here we explore the impact of calibration choice on KM5c SST data, by comparing and contrasting outputs between proxies and between calibrations. Although the TEX<sub>86</sub> proxy (Schouten et al., 2002) has also been used to generate mid-Piacenzian SSTs (e.g. O'Brien et al., 2014; Petrick et al., 2015; Rommerskirchen et al., 2011), these data are not included here because they could not be confidently assigned to the KM5c interval either due to low sampling resolution and/or because our age control protocol was not met.

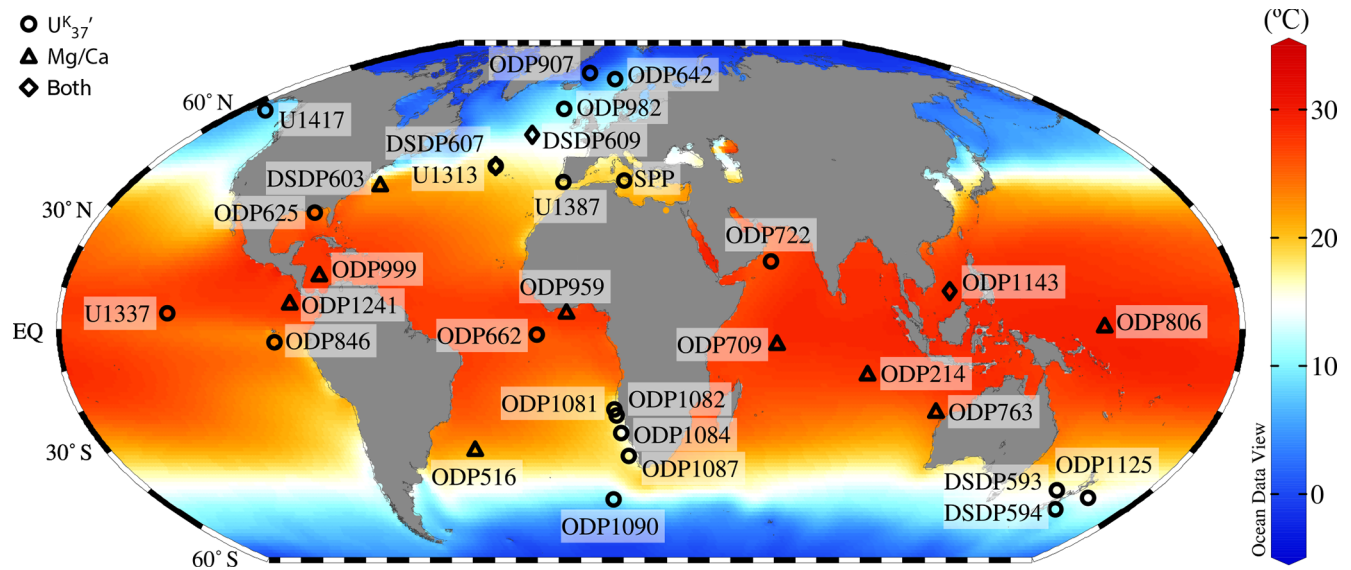


**Figure 2.** Locations of sites used in the synthesis, overlain on mean annual SST data from the World Ocean Atlas 2018 (Locarnini et al., 2018). A full list of the data sources and proxies applied per site are available in Tables S3 ( $U_{37}'$ ) and S4 (Mg/Ca) in the Supplement and can be accessed at <https://pliovar.github.io/km5c.html> (last access: 30 June 2020). The combined PlioVAR proxy data and their sources are also archived at Pangaea: <https://doi.pangaea.de/10.1594/PANGAEA.911847>.

### 2.3.1 Alkenone SSTs (the $U_{37}'$ index)

The majority of the 23 alkenone-derived SST datasets included in the PlioVAR synthesis used the  $U_{37}'$  index and applied the linear core-top calibration (60° S–60° N) (Müller et al., 1998) (hereafter Müller98; Tables S2 and S3). The Müller98 calibration applies the best fit between core-top  $U_{37}'$  and modern SSTs, recorded at the sea surface (0 m water depth) and consistent with haptophyte productivity in the photic zone. The sedimentary signal is proposed to record annual mean SST based on linear regression (Müller et al., 1998). Cultures of one of the dominant haptophytes, *Emiliania huxleyi*, generated only minor differences in the slope of the  $U_{37}'$ –temperature relationship (Table S2), where growth temperature was used for calibration (Prah et al., 1988). Several PlioVAR datasets were originally published using the Prah et al. (1988) calibration (Table S3).

A recent expansion of the global core-top database (< 70° N) was accompanied by Bayesian statistical analysis to assess the relationship(s) between predicted (from  $U_{37}'$ ) and recorded ocean temperatures (Tierney and Tingley, 2018). The revised  $U_{37}'$  calibration, BAYSPLINE, addresses non-linearity in the  $U_{37}'$ –SST relationship at the high end of the calibration, i.e. in the low-latitude oceans (Pelejero and Calvo, 2003; Sonzogni et al., 1997). BAYSPLINE also highlights scatter between predicted and observed SSTs at the high latitudes and explicitly reconstructs seasonal SSTs > 45° N (Pacific) and > 48° N (Atlantic) and in the Mediterranean Sea (Tierney and Tingley, 2018).

To test the impact of different alkenone temperature calibrations on the quantification of mid-Piacenzian SSTs, we

converted all  $U_{37}'$  data to SSTs using both the Müller98 calibration and the BAYSPLINE calibration. For most sites, BAYSPLINE was run with the recommended setting for the prior standard deviation scalar (pstd) of 10 (Tierney and Tingley, 2018). At high  $U_{37}'$  values (above ~ 24 °C) it is recommended to use the more restrictive value of 5, to minimise the possibility of generating unrealistic SSTs (e.g. > 40 °C) given that the slope of the  $U_{37}'$ –temperature calibration becomes attenuated (Tierney and Tingley, 2018).

### 2.3.2 Foraminifera Mg/Ca

The magnesium-to-calcium ratio of foraminifera calcite can be used to reconstruct sea-surface (surface dwelling), thermocline (subsurface dwelling), and deep (benthic) ocean temperatures (Delaney et al., 1985; Elderfield et al., 1996; Rosenthal et al., 1997). The PlioVAR dataset includes analysis from 12 sites, on surface-dwelling foraminifera *Globigerinoides ruber*, *Trilobatus sacculifer*, and *Globigerina bulloides* (Table S4). In the original publications, data were converted to SST using a range of calibrations as well as corrections for  $\text{CaCO}_3$  dissolution in the water column and sediments, which leads to preferential removal of Mg from the  $\text{CaCO}_3$  lattice (generating cooler SSTs than expected; Dekens et al., 2002; Regenberg et al., 2006, 2009). The evolution of the Mg/Ca of seawater ( $\text{Mg}/\text{Ca}_{\text{seawater}}$ ) over geological timescales may also impact Mg/Ca-based palaeo-temperature reconstructions (Brennan et al., 2013; Coggon et al., 2010; Fantle and DePaolo, 2005; Gothmann et al., 2015; Horita et al., 2002; Lowenstein et al., 2001). Changes in  $\text{Mg}/\text{Ca}_{\text{seawater}}$  impact the intercept and potentially the sen-



sitivity of palaeotemperature equations (Evans and Müller, 2012; Medina-Elizalde and Lea, 2010), but there remains uncertainty over the magnitude of Mg/Ca<sub>seawater</sub> changes in the late Pliocene (O'Brien et al., 2014; Evans et al., 2016).

To test the impact of different foraminifera Mg/Ca SST calibrations on mid-Piacenzian SSTs, we compare published SSTs with the recently developed BAYMAG calibration (Tierney et al., 2019b). We use published SSTs because the original researchers used their best judgement to choose a particular Mg/Ca-SST calibration, given that it (i) fitted modern (regional) core-top values; (ii) accounted for known environmental impacts (e.g. [CO<sub>3</sub><sup>2-</sup>] correction); (iii) was developed within a particular research group; and/or (iv) fitted conventional wisdom at the time. BAYMAG uses a Bayesian approach that incorporates laboratory culture and core-top information to generate probabilistic estimates of past temperatures. BAYMAG assumes a sensitivity of Mg/Ca to salinity, pH, and saturation state at each core site and also accounts for Mg/Ca<sub>seawater</sub> evolution through a linear scaling (i.e. there is no change in the sensitivity of the palaeotemperature equation as Mg/Ca<sub>seawater</sub> evolves) (Tierney et al., 2019b). For each site with Mg/Ca data, we computed SSTs using BAYMAG's species-specific hierarchical model. In the absence of knowledge concerning changes in salinity, pH, and saturation state in the Pliocene, we assumed that these values were the same as today. We drew seasonal sea-surface salinity from the World Ocean Atlas 2013 product (Boyer et al., 2013) and pH and bottom water saturation state from the GLODAPv2 product (Lauvset et al., 2016; Olsen et al., 2016). We used a prior standard deviation of 6 °C for all sites.

## 2.4 Climate models

The model outputs used here were generated from the 15 models that contribute to the Pliocene modelling intercomparison project, Phase 2 (PlioMIP2) (Haywood et al., 2020). The boundary conditions for the experiments and their large-scale results for Pliocene and pre-industrial climates are detailed elsewhere (Haywood et al., 2020, 2016b), so they are briefly outlined here.

The Pliocene simulations are intended to represent KM5c (~ 3.205 Ma) and were forced with PRISM4 boundary conditions (Haywood et al., 2016b). Atmospheric CO<sub>2</sub> concentration was set to 400 ppmv (Haywood et al., 2020), in line with the upper estimates of atmospheric CO<sub>2</sub> from boron isotope data (Fig. 1; Foster et al., 2017). Lower estimates from the alkenone carbon isotope proxy (Fig. 1) are likely to reflect an insensitivity of this proxy to atmospheric CO<sub>2</sub> in the Pliocene (Badger et al., 2019). All other trace gases, orbital parameters, and the solar constant were specified to be consistent with each model's pre-industrial experiment. The Greenland Ice Sheet was confined to high elevations in the eastern Greenland mountains, covering an area approximately 25 % of the present-day ice sheet. The Antarctic ice

sheet has no ice over West Antarctica. The reconstructed PRISM4 ice sheets have a total volume of  $20.1 \times 10^6 \text{ km}^3$ , equating to a sea-level increase relative to the present day of less than ~ 24 m (Dowsett et al., 2016).

Modelling groups had some choices regarding the exact implementation of boundary conditions; however, 14 of the 15 models used the “enhanced” PRISM4 boundary conditions (Dowsett et al., 2016) which included all reconstructed changes to the land–sea mask and ocean bathymetry. Key ocean gateway changes relative to modern values are the closure of the Bering Strait and Canadian archipelago, and the exposure of the Sunda and Sahul shelves (Dowsett et al., 2016). The initialisation of the experiments varied between models (Haywood et al., 2020). Some models were initialised from a pre-industrial state while others were initialised from the end of a previous Pliocene simulation or another warm state. The simulations reached equilibrium towards the end of the runs as per PlioMIP2 protocol.

## 2.5 Statistical analysis (calculating of global means and meridional gradients)

For all anomaly calculations we obtain pre-industrial SST from the NOAA-ERSST5 dataset for the years 1870–1899 CE (Huang et al., 2017), ensuring alignment between the KM5c proxy data and the KM5c model experiments (Haywood et al., 2020). This pre-industrial time window excludes the largest cooling linked to the Little Ice Age and predates the onset of 20th-century warming (Owens et al., 2017; PAGES2k Consortium, 2017). The global mean SST anomaly from the proxy data was obtained as follows: firstly, the SST anomaly between the proxy data and the NOAA-ERSST5 data was obtained for each location and the data collated into bins of 15° of latitude. It is assumed that the average of all the data in each bin represents the average SST anomaly for that latitude band. Next, the area of the ocean surface for each bin is obtained. The average SST anomaly is then the average of all the bins weighted by the ocean area in the relevant latitude band.

Meridional gradients were obtained in a similar way. A low-latitude SST anomaly was obtained as the weighted average of all the bins containing low-latitude SSTs (for example the 4° × 15° bins containing latitudes of 30° S–30° N). A high-latitude SST anomaly was obtained as the weighted average of all bins containing high-latitude SSTs (> 60° N because there were no proxy data points > 60° S). As only the Atlantic Ocean contained data points poleward of 65° N, the high-latitude region used in the gradient calculations for both proxies and models was focused on the longitudinal window from 70° W to 5° E. The meridional gradient SST anomaly is then the low-latitude SST anomaly minus the high-latitude SST anomaly, relative to the pre-industrial period.

There are some uncertainties in this calculation of the global mean SST, in particular, the fact that the proxy data are not evenly distributed throughout a latitude bin and also

that some bins contain very few data points. There is a higher density of data in the Atlantic Ocean compared to the Indian Ocean and Pacific Ocean, and no high-latitude data are available to consider a Southern Ocean response (Fig. 2). Nevertheless, this method of calculating averages does attempt to account for unevenly distributed data and provides an SST anomaly (SSTA) that is comparable with model results. The impact of proxy choice was examined in the calculation of the global means and meridional SST gradients. As no Mg/Ca data were available  $> 50^\circ \text{N}$  or  $> 30^\circ \text{S}$ , we calculated global mean SST and the meridional SST gradients either including or excluding the Mg/Ca data; both results are outlined below and shown in Table 1.

### 3 Results

Relative to the pre-industrial period, the combined  $U_{37}^{K'}$  and Mg/Ca proxy data, using the original calibrations, indicate a KM5c global mean SST anomaly of  $+2.3^\circ \text{C}$  and a meridional SST gradient reduced by  $2.6^\circ \text{C}$  (Fig. 3). The amplitude of the global SST mean anomaly in the combined proxy data exceeds those indicated in 10 of the PlioMIP2 models but is lower than the global SST anomaly from 6 models. The meridional temperature gradient anomalies are more comparable (Fig. 3). If only the  $U_{37}^{K'}$  data are used, the global mean SST anomaly from proxies is higher than all but three of the PlioMIP2 models, and the  $U_{37}^{K'}$  meridional gradient calculations are smaller than all models (BAYSPLINE) or one model (original calibration; Fig. 3).

Overall, the proxy data show the lowest temperature anomalies in the low latitudes, regardless of proxy (from  $+3$  to  $-4^\circ \text{C}$  for sites  $< 30^\circ \text{N/S}$ ). A larger range of temperature anomalies is reconstructed in the mid-latitudes and high latitudes (from  $+9$  to  $-2^\circ \text{C}$  for sites  $> 30^\circ \text{N/S}$ ) (Fig. 4). Thus, there is a broad, but complex, pattern of enhanced warming at the mid-latitudes and high latitudes, reflecting a combination of regional influences on circulation patterns and, to some extent, proxy choice. This pattern is not explained by temporal variability nor sample density within the KM5c time interval: regardless of sample number per site, the standard deviation at any site within the KM5c time bin is  $< 1.5^\circ \text{C}$  (Fig. S4 in the Supplement). We note that of the 32 sites examined here, 7 provided a single data point for the KM5c interval (Fig. S2, alkenones: ODP Sites 907, 1081, U1337, U1417; Fig. S3, foraminifera Mg/Ca: DSDP sites 214, 709, 763); the sites are geographically well distributed, however, and so unlikely to significantly impact our global mean/gradient calculations.

Calibration choice has a small impact over the reconstructed patterns of KM5c SST anomalies (Figs. 4, S2, and S3). Below  $24^\circ \text{C}$ , absolute  $U_{37}^{K'}$  SSTs using Müller98 are  $< 1^\circ \text{C}$  lower than those using BAYSPLINE. At high temperatures the non-linearity in the BAYSPLINE calibration means that BAYSPLINE SSTs can be up to  $1.67^\circ \text{C} \pm 0.01^\circ \text{C}$

higher than when using Müller98 (Fig. S2). The low-latitude offset between Müller98 and BAYSPLINE has two effects: it elevates the global mean SST (Fig. 3, Table 1) and increases the KM5c meridional SST gradient towards pre-industrial values (Figs. 3 and 4, Table 1). The calibration offsets are less systematic for Mg/Ca. There is a wider range of offsets between BAYMAG and published SST values (from  $-4$  to  $+5^\circ \text{C}$ ; Fig. S3, Table S3), although the smallest KM5c SST anomalies continue to be reconstructed in the low latitudes, regardless of which Mg/Ca calibration is applied (Fig. 4).

Overall, the  $U_{37}^{K'}$ -temperature anomalies lie within the range given by PlioMIP2 models (Fig. 4). The Mg/Ca estimates are mainly from the low latitudes, and high-latitude ( $> 60^\circ \text{N/S}$ ) Mg/Ca SST data are not available to calculate meridional gradients using foraminifera data alone (Fig. 4). Mg/Ca-SST anomalies are generally lower than for  $U_{37}^{K'}$ , and a cooler KM5c than the pre-industrial period is consistently (but not always) recorded in the low latitudes by Mg/Ca regardless of calibration choice (Fig. 4). As a result, combining  $U_{37}^{K'}$  and Mg/Ca data leads to a cooler global mean SST ( $\sim 2.3^\circ \text{C}$ ) than when using  $U_{37}^{K'}$  alone ( $\sim 3.2^\circ \text{C}$  with Müller98,  $\sim 3.4^\circ \text{C}$  with BAYSPLINE; Fig. 3 and Table 1). At eight sites, the negative KM5c SST anomalies in Mg/Ca disagree with both the  $U_{37}^{K'}$  data and the PlioMIP2 model outputs (Fig. 4). The disagreement is present regardless of whether the Müller98 or BAYSPLINE calibrations are applied, but the difference is larger in the low latitudes for BAYSPLINE because here this calibration generates higher SST values (Sect. 2.3.1). Only three sites have both  $U_{37}^{K'}$  and Mg/Ca data (DSDP Site 609, IODP sites U1313 and U1143) to enable direct comparison between Mg/Ca and alkenone SST data. Reconstructed SSTs for IODP sites U1313 and U1143 are within calibration uncertainty. At Site U1313 ( $41^\circ \text{N}$ ) there is overlap between both alkenone outputs (Müller98  $21.6^\circ \text{C}$ , BAYSPLINE  $20.9^\circ \text{C}$ ) and the original Mg/Ca reconstruction ( $22.2^\circ \text{C}$ ), whereas BAYMAG generates warmer SSTs ( $27.0^\circ \text{C}$ ). At Site 1143 ( $9^\circ \text{N}$ ), BAYSPLINE SSTs are warmer ( $30.6^\circ \text{C}$ ) than from the Müller98 ( $28.9^\circ \text{C}$ ), original Mg/Ca ( $27.7^\circ \text{C}$ ), and BAYMAG ( $27.1^\circ \text{C}$ ) calibrations. In contrast, DSDP Site 609 ( $49^\circ \text{N}$ ) has colder Mg/Ca estimates (original  $11.7^\circ \text{C}$ , BAYMAG  $12.5^\circ \text{C}$ ) than alkenones (Müller98  $17.7^\circ \text{C}$ , BAYSPLINE  $17.1^\circ \text{C}$ ) or models (Fig. 4).

## 4 Discussion

### 4.1 SST expression of the KM5c interglacial

KM5c is characterised by a surface ocean which is  $\sim 2.3^\circ \text{C}$  (alkenones and Mg/Ca),  $\sim 3.2^\circ \text{C}$  (alkenones-only, Müller98 calibration), or  $\sim 3.4^\circ \text{C}$  (alkenones-only, BAYSPLINE calibration) warmer than pre-industrial values, with a  $\sim 2.6^\circ \text{C}$  reduction in the meridional SST gradient. The global mean SST anomaly is higher than the  $1.7^\circ \text{C}$  previously calculated for the wider mid-Piacenzian warm period (3.1–3.3 Ma), regardless of proxy choice (IPCC, 2014b). Previous analysis

**Table 1.** Comparison of the magnitude of the global SST anomaly and meridional SST gradients between KM5c and the pre-industrial period, depending on proxy combination, and the latitudinal bands used for the gradient calculations.

Proxy	Global mean SST anomaly, °C	Meridional SST gradient anomaly, °C		
		30° S–30° N minus > 60° N	0–30° N minus > 60° N	15° S–15° N minus > 45° N/S
U <sub>37</sub> <sup>K'</sup> (original)	3.24	−1.18	−3.00	−1.56
U <sub>37</sub> <sup>K'</sup> (BAYSPLINE)	3.41	0.03	−1.66	−0.18
U <sub>37</sub> <sup>K'</sup> (original) + Mg/Ca	2.32	−2.61	−4.08	−2.84
U <sub>37</sub> <sup>K'</sup> (BAYSPLINE) + Mg/Ca (BAYMAG)	2.28	−2.21	−3.13	−2.19

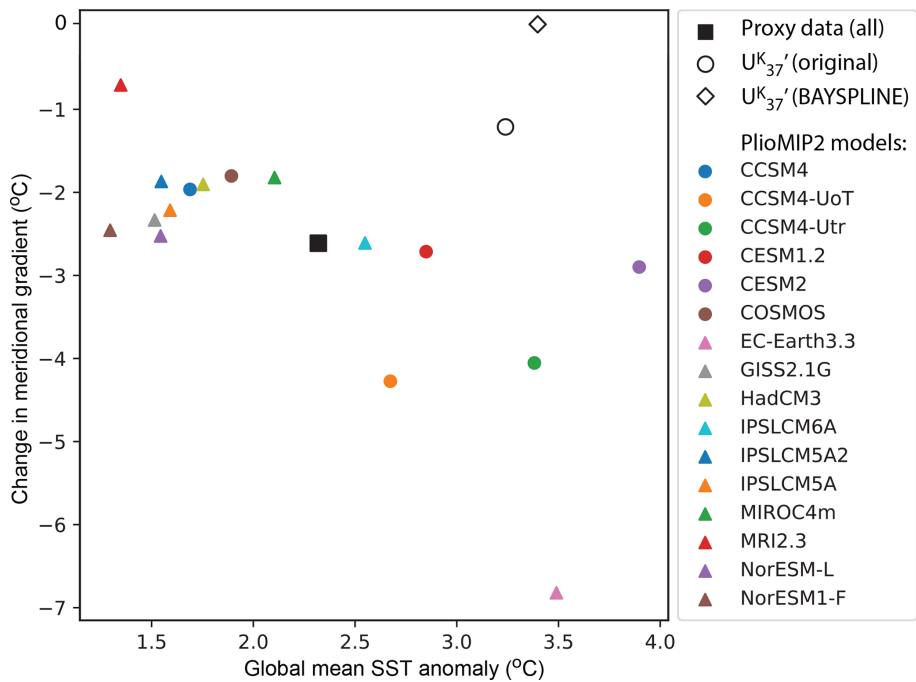


**Figure 3.** Comparison of KM5c SST data relative to the pre-industrial period (NOAA-ERSST5) for global mean SST anomalies (SSTA) and the change in meridional SST gradient, constructed using proxy data and the suite of PlioMIP2 models. Details of the model experiments are outlined in Table 1 of Haywood et al. (2020). The meridional SST gradient is calculated as 30° S–30° N minus 60–75° N, so that a more negative change in the gradient reflects a larger warming anomaly at high latitudes relative to low latitudes. As we only had data points poleward of 65° N in the Atlantic Ocean, the high-latitude region for both proxy and model gradient calculations focuses on the longitudinal window from 70° W to 5° E. Proxy data calculations were made using either all proxy data (U<sub>37</sub><sup>K'</sup> and Mg/Ca using their original calibrations) or using only U<sub>37</sub><sup>K'</sup> data and comparing the original and BAYSPLINE calibrations. No Mg/Ca data are available > 60° N, so we were unable to calculate Mg/Ca-only gradients (Fig. 4). The impact of changing the low- and high-latitude bands is explored in Table 1.

of a suite of models suggested that a climate state resembling the mid-Piacenzian was likely to develop and be sustained under RCP4.5 (Burke et al., 2018). The PlioMIP2 ensemble (Haywood et al., 2020) indicates that best estimates for mid-Piacenzian warming in surface air temperatures (1.7–5.2°) are comparable to projections for the RCP4.5 to 8.5 scenarios by 2100 CE (RCP4.5 = 1.8 ± 0.5°, RCP8.5 = 3.7 ± 0.7 °C; IPCC, 2013). Our proxy-based mean global SST anomaly is larger than in most PlioMIP2 mod-

els when we use only alkenones or alkenones and Mg/Ca combined (Fig. 3), and hence our results suggest that the global annual surface air temperature anomaly for KM5c would exceed the PlioMIP2 multi-model surface air temperature mean of 2.8 °C (Haywood et al., 2020). The higher global SST mean recorded in the KM5c proxy data, compared to the PlioMIP2 models, occurs despite the available atmospheric CO<sub>2</sub> reconstructions indicating values below the ~ 400 ppmv used in the PlioMIP2 models (Fig. 1). Our syn-



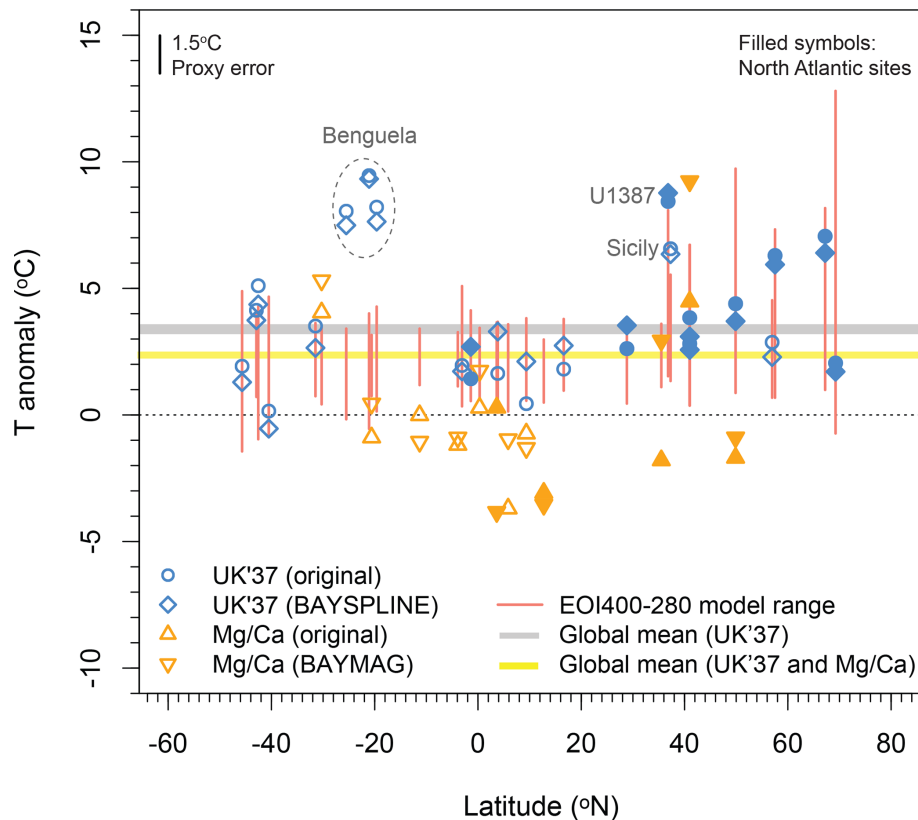


**Figure 4.** Reconstructed and modelled SST anomalies plotted by latitude. SST reconstructions using the original published data and two Bayesian approaches (BAYSPLINE, BAYMAG) are shown. The anomalies are calculated with reference to the NOAA-ERSST5 data for the years 1870–1899 CE at each site. Vertical red lines show the range of modelled annual SSTs from all PlioMIP2 experiments (Haywood et al., 2020) calculated at the grid boxes containing each site.

thesis of SST data thus indicates that with atmospheric  $\text{CO}_2$  concentrations  $\leq 400$  ppmv (comparable to RCP4.5), the surface ocean warming response will likely be larger than indicated in models. Further work is required to increase the temporal resolution of the atmospheric  $\text{CO}_2$  reconstructions through KM5c, to improve our understanding of the reconstructed SST response to  $\text{CO}_2$  forcing, including whether (or by how much) the reconstructed atmospheric  $\text{CO}_2$  differs from model boundary conditions and whether other changes in the model boundary conditions also influence SST patterns (e.g. gateway changes outlined in Sect. 2.4).

Proxy choice, calibration choice, and site selection have all had an impact on the magnitude of the change in meridional SST gradient for KM5c compared to the pre-industrial period (Table 1). Focussing only on a Northern Hemisphere SST gradient leads to higher gradient anomalies than when all of the low latitudes are included ( $30^\circ\text{S}$ – $30^\circ\text{N}$ ) because it excludes the high SST anomalies of the Benguela upwelling sites ( $20$ – $25^\circ\text{S}$ ; discussed below, Fig. 4). Smaller meridional SST gradient anomalies occur using BAYSPLINE ( $+0.03$  to  $-1.66^\circ\text{C}$ ) than the Müller98 calibration for  $\text{U}_{37}^K$  ( $-1.18$  to  $-3.00^\circ\text{C}$ ; Table 1), due to the increased low-latitude SST anomalies generated by BAYSPLINE (Fig. 4). Due to sev-

eral (but not all) low-latitude sites recording negative SST anomalies for KM5c using foraminifera Mg/Ca, the inclusion of Mg/Ca data leads to a larger difference in the meridional SST gradient relative to the pre-industrial period ( $-2.19$  to  $-4.08^\circ\text{C}$ ). Further work is required to fully understand the negative KM5c SST anomalies in some of the low-latitude sites (discussed further below), given their impact on the meridional SST gradients. However, a robust pattern emerging from the data is that the KM5c proxy data detail smaller low-latitude SST anomalies than those of the mid- and high-latitude SST anomalies (Fig. 4), leading to a reduction in the meridional SST gradient relative to the pre-industrial period. Enhanced mid- and high-latitude warming has been observed in other warm intervals of the geological past, including the last interglacial and the Eocene (Evans et al., 2018; Fischer et al., 2018), and is a feature of future climate under elevated  $\text{CO}_2$  concentrations (IPCC, 2014a).

There is complexity in the amplitude of the KM5c SST anomaly by latitude and basin, which may reflect patterns of surface ocean circulation. In the Northern Hemisphere, relatively muted warming in the East Greenland Current (ODP Site 907,  $69^\circ\text{N}$ ) may reflect the presence of at least seasonal sea-ice cover from ca. 4.5 Ma (Clotten et al., 2018). In con-

trast, relatively high SST anomalies at ODP Sites 642 (67° N) and 982 (58° N) track the northward flow of the North Atlantic Current, accounting for the enhanced warming relative to north-east Pacific IODP Site U1417 (57° N; Figs. 4 and 5). The large North Atlantic SST anomalies also contribute to an enhanced Northern Hemisphere meridional SST gradient of up to 4 °C (> 60° N minus 0–30° N; Table 1). For the Southern Hemisphere, a signal of polar amplification is less clearly identified than for the Northern Hemisphere (Fig. 4), although we recognise that all sites are < 46° S. Low KM5c SST anomalies (< 2 °C) at DSDP sites 593 and 594 (41 and 46° S, respectively) might be accounted for by a similar positioning of the Subtropical Front close to New Zealand during KM5c as today (McClymont et al., 2016; Caballero-Gill et al., 2019). Antarctic Intermediate Water (AAIW) temperatures were also only ~ 2.5 °C warmer than pre-industrial values during KM5c, suggesting a small warming in subantarctic waters where AAIW forms (McClymont et al., 2016). In contrast, large anomalies at ODP Sites 1125 (43° S, Pacific) and 1090 (43° S, Atlantic) reflect a greater sensitivity to expanded subtropical gyres during KM5c, contrasting with the Pleistocene equatorward displacement (and enhanced cooling) of subpolar water masses (e.g. Martinez-Garcia et al., 2010) which today places both of these sites poleward of the Subtropical Front.

Given that our proxy data meridional SST gradient calculations use only two sites to calculate the high-latitude SSTs (ODP Sites 907 and 642), which are also both from the Nordic Seas (Fig. 2), we explored the impact of expanding our high-latitude band into the mid-latitudes. We also explored narrowing the low-latitude band so that it does not include the Benguela upwelling sites, which have a significant data–model offset (Fig. 4) and may be influenced by localised circulation changes (see Sect. 4.2). Previous calculations of Pliocene meridional SST gradients have also considered differences between the mid-latitudes and low latitudes through time (Fedorov et al., 2015). Despite adding four more sites by expanding the high-latitude band to 45° N/S, the meridional SST gradients are reduced by < 0.4 °C, from –1.18 to –1.56 °C using the original  $U_{37}^{K'}$  data (Table 1). However, it is clear from the distribution of sites (Fig. 2) that our reconstructed KM5c SSTs (and thus the global mean and meridional gradients) have a strong signal from the Atlantic Ocean. There is a relative scarcity of sites from the Indian Ocean, Pacific Ocean, and Southern Ocean, but it is difficult to ascertain what impact this may have had on our global analysis. Further work is required to increase the spatial density of SST data for KM5c and the wider mid-Piacenzian stage, to better evaluate the magnitude of the warming and gradient changes outlined here.

#### 4.2 Proxy data–model comparisons for mid- and high-latitude sites

For the mid-latitudes and high latitudes, we find broad proxy data–model agreements for most sites. In the North Atlantic Ocean, reconstructed SST KM5c anomalies from  $U_{37}^{K'}$  fall within the ranges provided by the PlioMIP2 models (Fig. 4) for all but one site (IODP Site U1387, 37° N). The overall  $U_{37}^{K'}$ –model agreement for the North Atlantic Ocean suggests that, as proposed by Haywood et al. (2013), a focus on a specific interglacial within the mid-Piacenzian provides an improved comparison to the climate being simulated by the PlioMIP2 models. Thus, some of the data–model mismatch in previous mid-Piacenzian syntheses (e.g. Dowsett et al., 2012) may have been due to the averaging of warm peaks which may not have been synchronous in time between sites and/or with the interval being modelled. Disagreements occur between proxies (North Atlantic Ocean) and between proxies and models (Benguela upwelling, Gulf of Cadiz, Mediterranean Sea) (Fig. 4). Here, we explore the potential causes for these offsets in turn.

The largely  $U_{37}^{K'}$ -derived data from the North Atlantic Ocean tend to align with the warmest model outputs (Fig. 4), and the  $U_{37}^{K'}$ -SST anomalies also tend to be larger than those from Mg/Ca. A challenge for understanding the cause(s) of the  $U_{37}^{K'}$ –Mg/Ca differences is that only two sites have data from both proxies, and these do not show a consistent signal. There is good correspondence between  $U_{37}^{K'}$  and the original published Mg/Ca SSTs for IODP Site U1313 (41° N), whereas at ODP Site 609 Mg/Ca SSTs (both calibrations) are between 4.6 and 6.1 °C cooler than  $U_{37}^{K'}$ . It has also been shown that the  $U_{37}^{K'}$ –Mg/Ca SST offset at Site 609 is not constant with time for the late Pliocene (Lawrence and Woodard, 2017). When using BAYMAG, warmer KM5c SSTs are reconstructed than the original published data at DSDP Site 603 and IODP Site U1313 (35 and 41° N; Fig. 4), but BAYMAG reconstructs SSTs only 0.8 °C warmer than the original published SSTs at Site 609. These mid-latitude North Atlantic Mg/Ca data are provided by *G. bulloides*, which may calcify at depth in the water column (e.g. Mortyn and Charles, 2003; Schiebel et al., 1997) and account for those sites where Mg/Ca reconstructions give lower reconstructed SSTs than from  $U_{37}^{K'}$  (Bolton et al., 2018; De Schepper et al., 2013). Alternatively, an offset between alkenones and Mg/Ca might be accounted for if there is a seasonal bias to the  $U_{37}^{K'}$  calibration (e.g. Conte et al., 2006; Schneider et al., 2010). Despite documented seasonality in alkenone production at high latitudes, it has been proposed that mean annual SSTs continue to be recorded by  $U_{37}^{K'}$  in sediments (Rosell-Melé and Prahl, 2013), as indicated by the original  $U_{37}^{K'}$  calibration (Müller et al., 1998). In contrast, BAYSPLINE explicitly assumes an autumn signal is recorded at Atlantic sites > 45° N (Tierney and Tingley, 2018). Despite these differences in interpretation, BAYSPLINE values for KM5c are < 0.7 °C cooler than

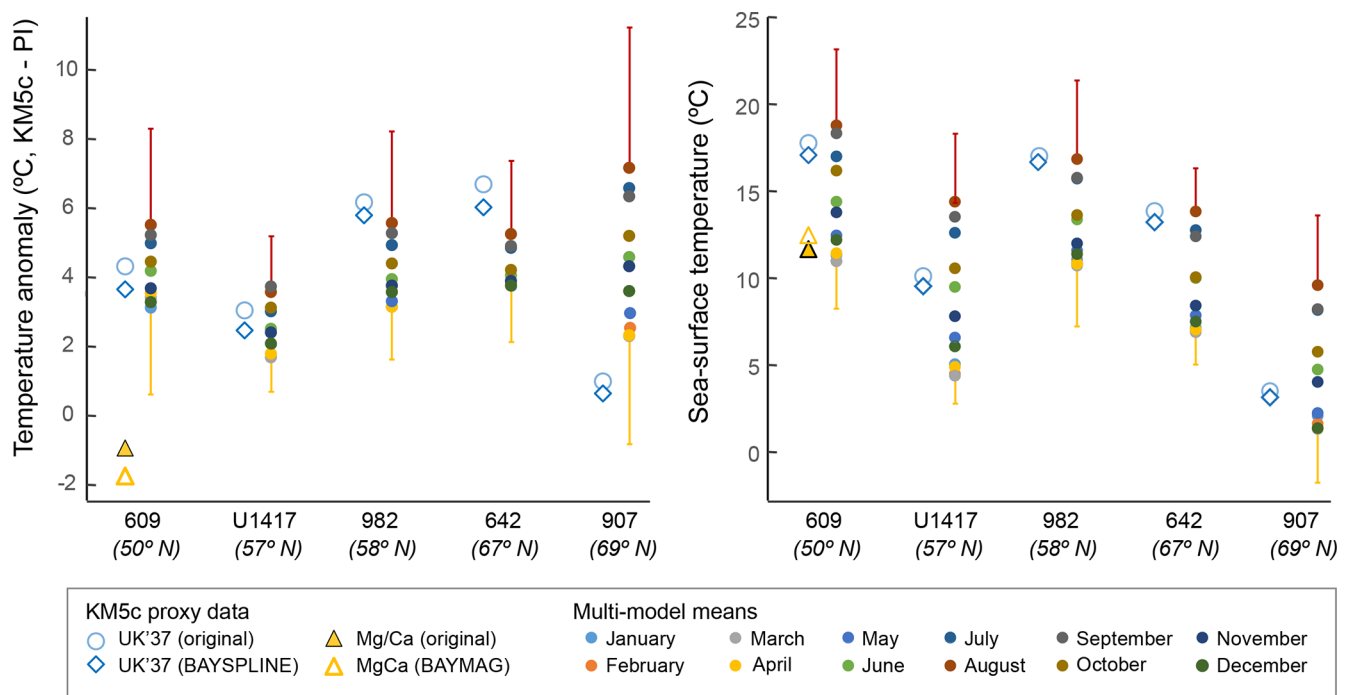


**Figure 5.** Investigating the potential seasonal signature recorded at high-latitude Northern Hemisphere sites ( $> 50^\circ \text{N}$ ), ordered by increasing latitude from left to right. Note that Site U1417 is from the North Pacific, where BAYSPLINE explicitly assumes that a summer signal is recorded  $> 48^\circ \text{N}$ . All other sites are from the Atlantic Ocean/Nordic Seas, where BAYSPLINE assumes an autumn signal  $> 45^\circ \text{N}$ . The original calibration by Müller et al. (1998) proposes that mean annual SSTs are recorded. Standard deviations of the multi-model means are shown for August (red) and April (yellow), which tend to be the maxima and minima, respectively.

the original published  $U_{37}^{K'}$  data (Fig. S2). Although the North Atlantic  $U_{37}^{K'}$  data align with a range of mean annual SST anomalies generated by the PlioMIP2 models (Fig. 4), three of the sites show alignment between  $U_{37}^{K'}$  SSTs and the July–November values from the multi-model means (Fig. 5). In contrast, Site 907 aligns with cool spring temperatures in the models, perhaps reflecting production after sea ice melt.

The large data–model discrepancy at  $30^\circ \text{S}$  reflects three sites which today sit beneath the Benguela upwelling system in the south-east Atlantic ( $20\text{--}26^\circ \text{S}$ ; Fig. 4). Part of the data–model discrepancy in the KM5c anomaly can be attributed to the models overestimating pre-industrial SSTs at the northern Benguela sites (NOAA-ERSST5 SSTs are  $2\text{--}5^\circ \text{C}$  below the pre-industrial model range) and suggests that models are not fully capturing the local dynamics of the coastal upwelling today (Small et al., 2015). Realistic representations of the Benguela upwelling system today are proposed to require realistic wind stress curl and high-resolution atmosphere and ocean models ( $< 1^\circ$ ; Small et al., 2015). Most of the PlioMIP2 simulations use lower-resolution atmosphere and ocean models (Haywood et al., 2020). An increased density of proxy data reconstructing KM5c atmospheric circulation, as well as the application of high-resolution models, may help to understand the observed KM5c data–model discrepancy. Furthermore, there was a deep thermocline during

the Pliocene (as reconstructed in the equatorial Pacific (Ford and Ravelo, 2019; Ford et al., 2015; Steph et al., 2006; Steph et al., 2010) and theorised globally (Philander and Fedorov, 2003)), so that warmer subsurface waters than today were upwelled, enhancing local warming. However, warming of  $\sim 3.4^\circ \text{C}$  in subsurface waters (Ford and Ravelo, 2019) and  $\sim 2.5^\circ \text{C}$  in intermediate waters (McClymont et al., 2016) for Pliocene interglacials suggests that Pliocene upwelling of warmer waters is unable to fully account for the  $7\text{--}10^\circ \text{C}$  SST anomalies at Benguela sites for KM5c. Changes to the distribution of export productivity and SSTs indicate that an overall poleward displacement of the Benguela upwelling system occurred during the Pliocene, so that the main zone of upwelling likely sat close to ODP Site 1087 at  $31^\circ \text{S}$  (Etourneau et al., 2009; Petrick et al., 2018; Rosell-Melé et al., 2014). As the northern and southern Benguela regions are today marked by differences in the seasonality of the upwelling, a temporal shift in upwelling intensity may also account for some of the large SST anomaly (Haywood et al., 2020). Thus, the data–model disagreement may be accounted for by a combination of displaced upwelling and warmer upwelled waters, giving large SST anomalies in Benguela proxy data, alongside the challenges of modelling both the pre-industrial and KM5c upwelling system and its associated SSTs.

Data–model disagreement also occurs at two Northern Hemisphere sites where  $U_{37}^{K'}$ -SST anomalies exceed those

given by the range of model predictions (Fig. 4). Punto Piccola (Sicily, 37° N) is located within the Mediterranean Sea, whereas IODP Site U1387 (37° N, Iberian margin) records the influence of the waters sourced from the Azores Current and the subtropical gyre. The data–model disagreement for KM5c reflects warmer SST estimates from the proxy data compared to the models, despite the good agreement for the pre-industrial period suggesting that locally complex ocean circulation in these near-shore and marginal marine settings may have been captured in the models. For Punto Piccola, the data–model offset is also likely to be a minimum because BAYSPLINE Mediterranean SSTs explicitly record November–May temperatures (Tierney and Tingley, 2018), and alkenone production below the sea surface has also been proposed (Ternois et al., 1997): both scenarios would act to raise mean annual SSTs further from those simulated in the PlioMIP2 models (Fig. 4). Further multi-proxy investigation is required to identify whether the data–model disagreements in the Benguela upwelling, Gulf of Cadiz, and Mediterranean Sea reflect challenges in modelling near-shore or complex oceanographic systems and/or biases in the temperature signal recorded by the proxy data.

#### 4.3 Data–model comparisons for low-latitude sites

The low-latitude  $U_{37}^{K'}$ -SST anomalies for KM5c align well with the PlioMIP2 models (Fig. 4). At ODP Sites 806 and 959, the Mg/Ca anomalies using the original calibrations are both +0.3 °C compared to the pre-industrial period (Fig. 4) and also align with the PlioMIP2 models. At Site 806 the BAYMAG KM5c anomaly (+1.7 °C) also aligns with the PlioMIP2 models. Only one low-latitude site has both  $U_{37}^{K'}$  and Mg/Ca SST data: ODP Site 1143 (9° N) records KM5c anomalies of +0.8 to +2.5 °C ( $U_{37}^{K'}$ ) or −0.7 to −1.3 °C (Mg/Ca). Although the  $U_{37}^{K'}$  data align with the model outputs for Site 1143, the negative anomaly in Mg/Ca lies outside the model range for mean annual SST (Fig. 4).

Six of the low-latitude sites have negative low-latitude SST anomalies in KM5c from foraminifera Mg/Ca; these occur regardless of whether the original or BAYMAG calibrations are applied and for both *G. ruber* and *T. sacculifer*-based reconstructions. The negative KM5c Mg/Ca-SST anomalies lie beyond those shown across the PlioMIP2 model range (Fig. 4), despite the absolute Mg/Ca SSTs reconstructed from these sites for KM5c falling within the model range for all but two of the sites (ODP Sites 999 (13° N) and 1241 (6° N); Fig. S5). However, the absolute SST values reconstructed for KM5c from Mg/Ca tend to align with the colder model outputs (Fig. S5).

Mg/Ca-SST calibration choice has no consistent impact on the KM5c anomalies (across all latitudes; Fig. 4). Therefore, the corrections for secular seawater Mg/Ca change and/or non-thermal influences over Mg/Ca, which are accounted for in BAYMAG (Tierney et al., 2019b), do not account for these cold tropical KM5c anomalies. For example,

for ODP Site 806 in the western Pacific warm pool, BAYMAG SST estimates for KM5c are ~ 1 °C warmer than the published Mg/Ca record (Wara et al., 2005). For Site 999 in the Caribbean Sea, BAYMAG SST estimates for KM5c are ~ 0.5 °C cooler than the published Mg/Ca record (De Schepper et al., 2013). This also suggests that the impact of Mg/Ca<sub>seawater</sub> change on SST is small on warm pool sites. The Mg/Ca<sub>seawater</sub> correction used in BAYMAG is conservative, drawing on multiple lines of physical evidence (corals, fluid inclusions, calcite veins, etc.) (Tierney et al., 2019b). Given the variable directions of the offsets between published and BAYMAG SSTs shown here, the Mg/Ca<sub>seawater</sub> correction is unable to account for the data–model offsets observed for the low latitudes.

CaCO<sub>3</sub> dissolution in the water column and sediments could lead to a cool bias on the Mg/Ca SSTs (Dekens et al., 2002; Regenberg et al., 2006, 2009). However, the cool KM5c anomalies also occur if the forward-modelled core-top Mg/Ca SSTs from BAYMAG are used as the pre-industrial “reference” (Fig. S6). The cold low-latitude anomalies for KM5c could reflect an increase in the calcification depth of the foraminifera, since the surface-dwelling foraminifera analysed here calcify at a range of depths, particularly in the tropics where the thermocline is deep in comparison to mid-latitudes to high latitudes (Fairbanks et al., 1982; Curry et al., 1983). The negative anomalies are broadly smaller for *G. ruber* (−0.4 to −1.2 °C) than for *T. sacculifer* (−0.6 to −3.5 °C), consistent with a deeper depth habitat for the latter (Curry et al., 1983), although at Site 959 the *G. ruber* anomaly using BAYMAG is −3.8 °C. There is therefore a lack of consistency between sites, which is difficult to resolve when single species have been analysed for each of the sites through KM5c.

Where there are very large differences between BAYMAG and published Mg/Ca SST estimates, regardless of latitude (e.g. North Atlantic; Fig. 4), we suggest that some combination of calibration difference, Mg/Ca<sub>seawater</sub> change, and/or other environmental factors including seasonality and calcification depth may offer an explanation. To fully investigate the cause(s) of offsets in Mg/Ca SST reconstructions requires future multi-species analysis for Mg/Ca for each site and multi-proxy analysis for each site. Such an approach would enable the exploration of a wider range of potential influences over both the Mg/Ca and  $U_{37}^{K'}$ -SST reconstructions and a reduction in the uncertainties of the reconstructed SSTs and their anomalies. Alongside foraminifera Mg/Ca and  $U_{37}^{K'}$  analyses, additional proxies which are likely to add valuable information about water column structure and seasonality could include TEX<sub>86</sub> (Schouten et al., 2002), long-chain diols (Rampen et al., 2012), and clumped isotopes (Tripathi et al., 2010). Previous research has demonstrated that even within a single site there can be offsets between proxies which are not continuous through time (e.g. Lawrence and Woodard, 2017; Petrick et al., 2018), so that high-resolution and multi-proxy work is required to fully understand the off-



sets we have identified here. Resolving the causes of the different proxy–proxy and proxy–model offsets is important because they impact the calculation of the global mean SST anomaly relative to pre-industrial values; however, even with the inclusion of the overall cooler Mg/Ca data, the combined KM5c proxy data still indicate a global mean SST anomaly which is larger than most models from the PlioMIP2 experiments (Fig. 3).

## 5 Conclusions

This study has generated a new multi-proxy synthesis of SST data for an interglacial stage (KM5c) from the Pliocene. By selecting an individual interglacial, with orbital forcing similar to modern values, we are able to focus on the SST response to atmospheric CO<sub>2</sub> concentrations comparable to today and the near future ( $\sim 400$  ppmv) but elevated relative to the pre-industrial period. Using strict stratigraphic protocols we selected only those data which could be confidently aligned to KM5c. By comparing different calibrations and two different proxy systems ( $U_{37}^{K'}$  and Mg/Ca in planktonic foraminifera) we identified several robust signals which are proxy-independent. First, global mean SSTs during KM5c were warmer than pre-industrial values. Second, there was a reduced meridional SST gradient which is the result of relatively small low-latitude SST anomalies and a larger range of warming anomalies for the mid-latitudes and high latitudes. Overall, there is good data–model agreement for both the absolute SSTs and the anomalies relative to the pre-industrial period, although there are complexities in the results. Further work is required to generate multi-proxy SST data from single sites, accompanied by robust reconstructions of thermocline temperatures using multi-species foraminifera analysis, so that the range of factors explaining proxy and calibration offsets can be explored more fully.

The choice of proxy for SST reconstruction impacts the overall calculation of global mean SST and the meridional gradients. The negative anomalies in Mg/Ca SSTs at 6 of the 16 low-latitude sites lowers the global mean SST of KM5c from  $\sim 3.2$ – $3.4$  °C ( $U_{37}^{K'}$ -only) to  $\sim 2.3$  °C (combined  $U_{37}^{K'}$  and Mg/Ca). The meridional SST gradient anomalies are decreased to  $-2.6$  °C (combined  $U_{37}^{K'}$  and Mg/Ca) relative to the pre-industrial period, although a more muted reduction (up to  $-1.18$  °C) occurs with  $U_{37}^{K'}$  alone. A number of factors may lead to a cool bias in the foraminifera Mg/Ca SSTs, which require further investigation through multi-proxy and multi-species analysis, particularly at low-latitude sites.

We identify the strongest warming across the North Atlantic region. The results are consistent with the PlioMIP2 models, although the largely  $U_{37}^{K'}$  data sit at the high end of the calculated model anomalies. Although seasonality may play a role in the proxy data signal, these results also suggest that many models may underestimate high-latitude warming even with the moderate CO<sub>2</sub> increases identified in KM5c

relative to the pre-industrial period. More data points are required to fully explore these patterns: for seven sites only one data point lay within KM5c, and more than half of the analysed sites (18/32) recorded Atlantic Ocean SSTs.

Both the PlioMIP2 models (Haywood et al., 2020) and future projections (IPCC, 2019) indicate that warming is higher over land than in the oceans in response to higher atmospheric CO<sub>2</sub> concentrations. Our synthesis of KM5c thus likely represents a minimum warming to be expected with atmospheric CO<sub>2</sub> concentrations of  $\sim 400$  ppmv. Even under low-CO<sub>2</sub> emission scenarios, our results demonstrate that surface ocean warming may be expected to exceed model projections and will be accentuated in the higher latitudes.

**Data availability.** The combined proxy data (absolute SST reconstructions and anomalies to the pre-industrial period) and full details of the data sources are available at <https://doi.org/10.1594/PANGAEA.911847> (McClymont et al., 2020).

**Supplement.** Additional information on proxy calibrations and their impact on the SST reconstructions is available in the supplement. The supplement related to this article is available online at: <https://doi.org/10.5194/cp-16-1599-2020-supplement>.

**Author contributions.** ELM, HLF, and SLH designed the data analysis and led the data compilation. JCT and AMH processed outputs from the suite of PlioMIP2 models, and calculated global means and meridional SST gradients using the proxy data. Proxy data were compiled and their age models reviewed by ELM, HLF, MAG, IB, KL, MP, BP, ACR, BR, SDS, GEAS, KT, and SW. Proxy calibrations were reviewed and applied by ELM, MAB, HLF, SLH, FP, JET, and CvdW. PlioMIP2 model experiments were designed and run and the outputs processed by AAO, MLJB, EB, WLC, DC, RF, CG, AMH, AvdH, SH, XL, GL, KHN, BLOB, WRP, CS, JCT, and ZZ. ELM, HLF, and SLH prepared the paper with contributions from all co-authors.

**Competing interests.** The authors declare that they have no conflict of interest.

**Special issue statement.** This article is part of the special issue “PlioMIP Phase 2: experimental design, implementation and scientific results”. It is not associated with a conference.

**Acknowledgements.** This work is an outcome from several workshops sponsored by Past Global Change (PAGES) as contributions to the working group on Pliocene Climate Variability over glacial-interglacial timescales (PlioVAR). We acknowledge PAGES for their support and the workshop participants for discussions. Funding support has also been provided

by NERC (NE/I027703/1 and NE/L002426/1 to Erin L. McClymont, NERC NE/N015045/1 to Heather L. Ford), Leverhulme Trust (Philip Leverhulme Prize, Erin L. McClymont), and the Research Council of Norway (Björg Risebrobakken and Erin L. McClymont (221712), Stijn De Schepper (229819)). Michiel L. J. Baatsen, Anna von der Heydt, Francien Peterse, and Carolien van der Weijst are part of the Netherlands Earth System Science Centre (NESSC), financially supported by the Dutch Ministry of Education, Culture and Science (OCW). Montserrat Alonso-Garcia acknowledges support from FCT (SFRH/BPD/96960/2013, PTDC/MAR-PRO/3396/2014, and CCMAR UID/Multi/04326/2019). W. Richard Peltier and Deepak Chandan were supported by Canadian NSERC Discovery Grant A9627, and they wish to acknowledge the support of SciNet HPC Consortium for providing computing facilities. SciNet is funded by the Canada Foundation for Innovation under the auspices of Compute Canada, the Government of Ontario, the Ontario Research Fund – Research Excellence, and the University of Toronto. Gerrit Lohmann and Christian Stepanek acknowledge funding by the Helmholtz Climate Initiative REKLIM and the Alfred Wegener Institute's research programme PACES2. Wing-Le Chan and Ayako Abe-Ouchi acknowledge funding from JSPS KAKENHI grant 17H06104 and MEXT KAKENHI grant 17H06323 as well as JAMSTEC for use of the Earth Simulator supercomputer. Bette L. Otto-Bliesner, Esther C. Brady, and Ran Feng acknowledge the CESM project, which is supported primarily by the National Science Foundation (NSF). This material is based upon work supported by the National Center for Atmospheric Research (NCAR), which is a major facility sponsored by the NSF under Cooperative Agreement No. 1852977. Computing and data storage resources, including the Cheyenne supercomputer (<https://doi.org/10.5065/D6RX99HX>), were provided by the Computational and Information Systems Laboratory (CISL) at NCAR. This research used samples and/or data provided by the International Ocean Discovery Program (IODP), Ocean Drilling Program (ODP), and Deep Sea Drilling Project (DSDP).

**Financial support.** This research has been supported by the NERC (grant nos. NE/I027703/1, NE/L002426/1, and NE/N015045/1), the Leverhulme Trust, the Research Council of Norway (grant nos. 221712 and 229819), the Dutch Ministry of Education, Culture and Science (OCW), FCT (grant nos. SFRH/BPD/96960/2013, PTDC/MAR-PRO/3396/2014, and CCMAR UID/Multi/04326/2019), a Canadian NSERC Discovery Grant (grant no. A9627), the Helmholtz Climate Initiative REKLIM, the Alfred Wegener Institute's research programme PACES2, JSPS KAKENHI (grant no. 17H06104), MEXT KAKENHI (grant no. 17H06323), and the National Science Foundation (NSF, CESM project; grant no. 1852977).

**Review statement.** This paper was edited by Aisling Dolan and reviewed by Antje Voelker and Tim Herbert.

## References

- Ahn, S., Khider, D., Lisiecki, L. E., and Lawrence, C. E.: A probabilistic Pliocene–Pleistocene stack of benthic  $\delta^{18}\text{O}$  using a profile hidden Markov model, *Dynamics and Statistics of the Climate System*, 2, dzx002, <https://doi.org/10.1093/climsys/dzx002>, 2017.
- Badger, M. P. S., Chalk, T. B., Foster, G. L., Bown, P. R., Gibbs, S. J., Sexton, P. F., Schmidt, D. N., Pälike, H., Mackensen, A., and Pancost, R. D.: Insensitivity of alkenone carbon isotopes to atmospheric CO<sub>2</sub> at low to moderate CO<sub>2</sub> levels, *Clim. Past*, 15, 539–554, <https://doi.org/10.5194/cp-15-539-2019>, 2019.
- Bolton, C. T., Bailey, I., Friedrich, O., Tachikawa, K., de Garidel-Thoron, T., Vidal, L., Sonzogni, C., Marino, G., Rohling, E. J., Robinson, M. M., Ermini, M., Koch, M., Cooper, M. J., and Wilson, P. A.: North Atlantic Midlatitude Surface-Circulation Changes Through the Plio-Pleistocene Intensification of Northern Hemisphere Glaciation, *Paleoceanography and Paleoclimatology*, 33, 1186–1205, <https://doi.org/10.1029/2018pa003412>, 2018.
- Boyer, T. P., Antonov, J. I., Baranova, O. K., Coleman, C., Garcia, H. E., Grodsky, A., Johnson, D. R., Locarnini, R. A., Mishonov, A. V., O'Brien, T. D., Paver, C. R., Reagan, J. R., Seidov, D., Smolyar, I. V., and Zweng, M. M.: World Ocean Database 2013, in: NOAA Atlas NESDIS 72, edited by: Levitus, S. and Mishonov, A., National Oceanic and Atmospheric Administration Ocean Climate Laboratory, Silver Spring, MD, 209 pp., <https://doi.org/10.7289/V5NZ85MT>, 2013.
- Brennan, S. T., Lowenstein, T. K., and Cendón, D. I.: The major-ion composition of Cenozoic seawater: The past 36 million years from fluid inclusions in marine halite, *Am. J. Sci.*, 313, 713–775, <https://doi.org/10.2475/08.2013.01>, 2013.
- Burke, K. D., Williams, J. W., Chandler, M. A., Haywood, A. M., Lunt, D. J., and Otto-Bliesner, B. L.: Pliocene and Eocene provide best analogs for near-future climates, *P. Natl. Acad. Sci. USA*, 115, 13288–13293, <https://doi.org/10.1073/pnas.1809600115>, 2018.
- Caballero-Gill, R. P., Herbert, T. D., and Dowsett, H. J.: 100-kyr Paced Climate Change in the Pliocene Warm Period, Southwest Pacific, *Paleoceanography and Paleoclimatology*, 34, 524–545, <https://doi.org/10.1029/2018pa003496>, 2019.
- Clotten, C., Stein, R., Fahl, K., and De Schepper, S.: Seasonal sea ice cover during the warm Pliocene: Evidence from the Iceland Sea (ODP Site 907), *Earth Planet. Sc. Lett.*, 481, 61–72, <https://doi.org/10.1016/j.epsl.2017.10.011>, 2018.
- Coggon, R. M., Teagle, D. A. H., Smith-Duque, C. E., Alt, J. C., and Cooper, M. J.: Reconstructing Past Seawater Mg/Ca and Sr/Ca from Mid-Ocean Ridge Flank Calcium Carbonate Veins, *Science*, 327, 1114–1117, <https://doi.org/10.1126/science.1182252>, 2010.
- Conte, M. H., Sicre, M.-A., Rühlemann, C., Weber, J. C., Schulte, S., Schulz-Bull, D., and Blanz, T.: Global temperature calibration of the alkenone unsaturation index ( $U_{37}^{K'}$ ) in surface waters and comparison with surface sediments, *Geochem. Geophys. Geosy.*, 7, Q02005, <https://doi.org/10.1029/2005GC001054>, 2006.
- Curry, W. B., Thunell, R. C., and Honjo, S.: Seasonal changes in the isotopic composition of planktonic foraminifera collected in Panama Basin sediment traps, *Earth Planet. Sc. Lett.*, 64, 33–43, [https://doi.org/10.1016/0012-821X\(83\)90050-X](https://doi.org/10.1016/0012-821X(83)90050-X), 1983.

- De Schepper, S., Groeneveld, J., Naafs, B. D. A., Van Renterghem, C., Hennissen, J., Head, M. J., Louwye, S., and Fabian, K.: Northern Hemisphere Glaciation during the Globally Warm Early Late Pliocene, *Plos One*, 8, e81508, <https://doi.org/10.1371/journal.pone.0081508>, 2013.
- Dekens, P. S., Lea, D. W., Pak, D. K., and Spero, H. J.: Core top calibration of Mg/Ca in tropical foraminifera: Refining paleotemperature estimation, *Geochem. Geophys. Geosy.*, 3, 1022, <https://doi.org/10.1029/2001GC000200>, 2002.
- Delaney, M. L., Be, A. W. H., and Boyle, E. A.: Li, Sr, Mg, and Na in foraminiferal calcite shells from laboratory culture, sediment traps, and sediment cores, *Geochim. Cosmochim. Ac.*, 49, 1327–1341, 1985.
- Dowsett, H. J., Robinson, M. M., Haywood, A. M., Hill, D. J., Dolan, A. M., Stoll, D. K., Chan, W.-L., Abe-Ouchi, A., Chandler, M. A., Rosenbloom, N. A., Otto-Bliesner, B. L., Bragg, F. J., Lunt, D. J., Foley, K. M., and Riesselman, C. R.: Assessing confidence in Pliocene sea surface temperatures to evaluate predictive models, *Nature Clim. Change*, 2, 365–371, 2012.
- Dowsett, H., Dolan, A., Rowley, D., Moucha, R., Forte, A. M., Mitrovica, J. X., Pound, M., Salzmann, U., Robinson, M., Chandler, M., Foley, K., and Haywood, A.: The PRISM4 (mid-Piacenzian) paleoenvironmental reconstruction, *Clim. Past*, 12, 1519–1538, <https://doi.org/10.5194/cp-12-1519-2016>, 2016.
- Elderfield, H., Bertram, C. J., and Erez, J.: A biomineralization model for the incorporation of trace elements into foraminiferal calcium carbonate, *Earth Planet. Sc. Lett.*, 142, 409–423, [https://doi.org/10.1016/0012-821X\(96\)00105-7](https://doi.org/10.1016/0012-821X(96)00105-7), 1996.
- Etourneau, J., Martinez, P., Blanz, T., and Schneider, R.: Pliocene-Pleistocene variability of upwelling activity, productivity, and nutrient cycling in the Benguela region, *Geology*, 37, 871–874, <https://doi.org/10.1130/g25733a.1>, 2009.
- Evans, D. and Müller, W.: Deep time foraminifera Mg/Ca paleothermometry: Nonlinear correction for secular change in seawater Mg/Ca, *Paleoceanography*, 27, PA4205, <https://doi.org/10.1029/2012pa002315>, 2012.
- Evans, D., Brierley, C., Raymo, M. E., Erez, J., and Müller, W.: Planktic foraminifera shell chemistry response to seawater chemistry: Pliocene–Pleistocene seawater Mg/Ca, temperature and sea level change, *Earth Planet. Sc. Lett.*, 438, 139–148, <https://doi.org/10.1016/j.epsl.2016.01.013>, 2016.
- Evans, D., Sagoo, N., Renema, W., Cotton, L. J., Müller, W., Todd, J. A., Saraswati, P. K., Stassen, P., Ziegler, M., Pearson, P. N., Valdes, P. J., and Affek, H. P.: Eocene greenhouse climate revealed by coupled clumped isotope-Mg/Ca thermometry, *P. Natl. Acad. Sci. USA*, 115, 1174–1179, <https://doi.org/10.1073/pnas.1714744115>, 2018.
- Fairbanks, R. G., Sverdrlove, M., Free, R., Wiebe, P. H., and Bé, A. W. H.: Vertical distribution and isotopic fractionation of living planktonic foraminifera from the Panama Basin, *Nature*, 298, 841–844, <https://doi.org/10.1038/298841a0>, 1982.
- Fantle, M. S. and DePaolo, D. J.: Variations in the marine Ca cycle over the past 20 million years, *Earth Planet. Sc. Lett.*, 237, 102–117, 2005.
- Fedorov, A. V., Burls, N. J., Lawrence, K. T., and Peterson, L. C.: Tightly linked zonal and meridional sea surface temperature gradients over the past five million years, *Nat. Geosci.*, 8, 975–980, <https://doi.org/10.1038/ngeo2577>, 2015.
- Feng, R., Otto-Bliesner, B. L., Fletcher, T. L., Tabor, C. R., Ballantyne, A. P., and Brady, E. C.: Amplified Late Pliocene terrestrial warmth in northern high latitudes from greater radiative forcing and closed Arctic Ocean gateways, *Earth Planet. Sc. Lett.*, 466, 129–138, 2017.
- Fischer, H., Meissner, K. J., Mix, A. C., Abram, N. J., Austermann, J., Brovkin, V., Capron, E., Colombaroli, D., Danian, A.-L., Dyez, K. A., Felis, T., Finkelstein, S. A., Jaccard, S. L., McClymont, E. L., Rovere, A., Sutter, J., Wolff, E. W., Affolter, S., Bakker, P., Ballesteros-Cánovas, J. A., Barbante, C., Caley, T., Carlson, A. E., Churakova, O., Cortese, G., Cumming, B. F., Davis, B. A. S., de Vernal, A., Emile-Geay, J., Fritz, S. C., Gierz, P., Gottschalk, J., Holloway, M. D., Joos, F., Kucera, M., Loutre, M.-F., Lunt, D. J., Marcisz, K., Marlon, J. R., Martinez, P., Masson-Delmotte, V., Nehrbass-Ahles, C., Otto-Bliesner, B. L., Raible, C. C., Risebrobakken, B., Sánchez Goñi, M. F., Arrigo, J. S., Sarnthein, M., Sjolte, J., Stocker, T. F., Velasquez Álvarez, P. A., Tinner, W., Valdes, P. J., Vogel, H., Wanner, H., Yan, Q., Yu, Z., Ziegler, M., and Zhou, L.: Palaeoclimate constraints on the impact of 2 °C anthropogenic warming and beyond, *Nat. Geosci.*, 11, 474–485, <https://doi.org/10.1038/s41561-018-0146-0>, 2018.
- Foley, K. M. and Dowsett, H. J.: Community sourced mid-Piacenzian sea surface temperature (SST) data, US Geological Survey data release, <https://doi.org/10.5066/P9YP3DTV>, 2019.
- Ford, H. L. and Ravelo, A. C.: Estimates of Pliocene Tropical Pacific Temperature Sensitivity to Radiative Greenhouse Gas Forcing, 34, 2–15, <https://doi.org/10.1029/2018pa003461>, 2019.
- Ford, H. L., Ravelo, A. C., Dekens, P., LaRiviere, J. P., and Wara, M.: The evolution of the equatorial thermocline and the early Pliocene El Padre mean state, *Geophys. Res. Lett.*, 42, 4878–4887, <https://doi.org/10.1002/2015GL064215>, 2015.
- Foster, G. L., Royer, D. L., and Lunt, D. J.: Future climate forcing potentially without precedent in the last 420 million years, *Nat. Commun.*, 8, 14845, <https://doi.org/10.1038/ncomms14845>, 2017.
- Gothmann, A. M., Stolarski, J., Adkins, J. F., Schoene, B., Dennis, K. J., Schrag, D. P., Mazur, M., and Bender, M. L.: Fossil corals as an archive of secular variations in seawater chemistry since the Mesozoic, *Geochim. Cosmochim. Ac.*, 160, 188–208, <https://doi.org/10.1016/j.gca.2015.03.018>, 2015.
- Gradstein, F. M., Schmitz, J. G., Ogg, M. D., and Ogg, G. M.: The Geological Time Scale 2012, Elsevier, <https://doi.org/10.1016/B978-0-444-59425-9.01001-5>, 2012.
- Haywood, A. M., Dolan, A. M., Pickering, S. J., Dowsett, H. J., McClymont, E. L., Prescott, C. L., Salzmann, U., Hill, D. J., Lunt, D. J., Pope, J. O., and Valdes, P. J.: On the identification of a Pliocene time slice for data-model comparison, *Philos. T. Roy. Soc. A*, 371, 20120515, <https://doi.org/10.1098/rsta.2012.0515>, 2013.
- Haywood, A. M., Dowsett, H. J., and Dolan, A. M.: Integrating geological archives and climate models for the mid-Pliocene warm period, *Nat. Commun.*, 7, <https://doi.org/10.1038/ncomms10646>, 2016a. Haywood, A. M., Dowsett, H. J., Dolan, A. M., Rowley, D., Abe-Ouchi, A., Otto-Bliesner, B., Chandler, M. A., Hunter, S. J., Lunt, D. J., Pound, M., and Salzmann, U.: The Pliocene Model Intercomparison Project (PlioMIP) Phase 2: scientific objectives and experimental design, *Clim. Past*, 12, 663–675, <https://doi.org/10.5194/cp-12-663-2016>, 2016b.

- Haywood, A. M., Tindall, J. C., Dowsett, H. J., Dolan, A. M., Foley, K. M., Hunter, S. J., Hill, D. J., Chan, W.-L., Abe-Ouchi, A., Stepanek, C., Lohmann, G., Chandan, D., Peltier, W. R., Tan, N., Contoux, C., Ramstein, G., Li, X., Zhang, Z., Guo, C., Nisancioglu, K. H., Zhang, Q., Li, Q., Kamae, Y., Chandler, M. A., Sohl, L. E., Otto-Bliesner, B. L., Feng, R., Brady, E. C., von der Heydt, A. S., Baatsen, M. L. J., and Lunt, D. J.: A return to large-scale features of Pliocene climate: the Pliocene Model Intercomparison Project Phase 2, *Clim. Past Discuss.*, <https://doi.org/10.5194/cp-2019-145>, in review, 2020.
- Hoffman, J. S., Clark, P. U., Parnell, A. C., and He, F.: Regional and global sea-surface temperatures during the last interglaciation, *Science*, 355, 276–279, <https://doi.org/10.1126/science.aai8464>, 2017.
- Horita, J., Zimmermann, H., and Holland, H. D.: Chemical evolution of seawater during the Phanerozoic: Implications from the record of marine evaporites, *Geochim. Cosmochim. Ac.*, 66, 3733–3756, [https://doi.org/10.1016/S0016-7037\(01\)00884-5](https://doi.org/10.1016/S0016-7037(01)00884-5), 2002.
- Huang, B., Thorne, P. W., Banzon, V. F., Boyer, T., Chepurin, G., Lawrimore, J. H., Menne, M. J., Smith, T. M., Vose, R. S., and Zhang, H.-M.: Extended Reconstructed Sea Surface Temperature, Version 5 (ERSSTv5): Upgrades, Validations, and Intercomparisons, *J. Climate*, 30, 8179–8205, <https://doi.org/10.1175/jcli-d-16-0836.1>, 2017.
- IPCC, Climate Change 2014: Synthesis Report. Contribution of Working Groups I, II and III to the Fifth Assessment Report of the Intergovernmental Panel on Climate Change, IPCC, Geneva, Switzerland, 151, 2014a.
- IPCC: Summary for policymakers, in: Climate Change 2014: Impacts, Adaptation, and Vulnerability. Part A: Global and Sectoral Aspects. Contribution of Working Group II to the Fifth Assessment Report of the Intergovernmental Panel on Climate Change, edited by: Field, C. B., Barros, V. R., Dokken, D. J., Mach, K. J., Mastrandrea, M. D., Bilir, T. E., Chatterjee, M., Ebi, K. L., Estrada, Y. O., Genova, R. C., Girma, B., Kissel, E. S., Levy, A. N., MacCracken, S., Mastrandrea, P. R., and White, L. L., Cambridge University Press, Cambridge, United Kingdom, and New York, NY, USA, 1–32, 2014b.
- IPCC: Global Warming of 1.5 °C. An IPCC Special Report on the impacts of global warming of 1.5 °C above pre-industrial levels and related global greenhouse gas emission pathways, in the context of strengthening the global response to the threat of climate change, sustainable development, and efforts to eradicate poverty, edited by: Masson-Delmotte, V., Zhai, P., Pörtner, H.-O., Roberts, D., Skea, J., Shukla, P. R., Pirani, A., Moufouma-Okia, W., Péan, C., Pidcock, R., Connors, S., Matthews, J. B. R., Chen, Y., Zhou, X., Gomis, M. I., Lonnoy, E., Maycock, T., Tignor, M., and Waterfield, T., available at: <https://www.ipcc.ch/srocc/> (last access: 8 August 2020), 2019.
- Lauvset, S. K., Key, R. M., Olsen, A., van Heuven, S., Velo, A., Lin, X., Schirnick, C., Kozyr, A., Tanhua, T., Hoppema, M., Jutterström, S., Steinfeldt, R., Jeansson, E., Ishii, M., Perez, F. F., Suzuki, T., and Watelet, S.: A new global interior ocean mapped climatology: the 1° × 1° GLODAP version 2, *Earth Syst. Sci. Data*, 8, 325–340, <https://doi.org/10.5194/essd-8-325-2016>, 2016.
- Lawrence, K. T. and Woodard, S. C.: Past sea surface temperatures as measured by different proxies—A cautionary tale from the late Pliocene, *Paleoceanography*, 32, 318–324, <https://doi.org/10.1002/2017pa003101>, 2017.
- Lisiecki, L. E. and Raymo, M. E.: A Pliocene-Pleistocene stack of 57 globally distributed benthic δ<sup>18</sup>O records, *Paleoceanography*, 20, PA1003, <https://doi.org/10.1029/2004PA001071>, 2005.
- Locarnini, R. A., Mishonov, A. V., Baranova, O. K., Boyer, T. P., Zweng, M. M., Garcia, H. E., Reagan, J. R., Seidov, D., Weathers, K., Paver, C. R., and Smolyar, I.: World Ocean Atlas 2018, Volume 1: Temperature, edited by: Mishonov, A., NOAA Atlas NESDIS 81, National Centers for Environmental Information, Silver Spring, MD, USA, 52 pp., 2018.
- Loulergue, L., Schilt, A., Spahni, R., Masson-Delmotte, V., Blunier, T., Lemieux, B., Barnola, J.-M., Raynaud, D., Stocker, T. F., and Chappellaz, J.: Orbital and millennial-scale features of atmospheric CH<sub>4</sub> over the past 800,000 years, *Nature*, 453, 383–386, 2008.
- Lowenstein, T. K., Timofeeff, M. N., Brennan, S. T., Hardie, L. A., and Demicco, R. V.: Oscillations in Phanerozoic Seawater Chemistry: Evidence from Fluid Inclusions, *Science*, 294, 1086–1088, <https://doi.org/10.1126/science.1064280>, 2001.
- Martinez-Garcia, A., Rosell-Mele, A., McClymont, E. L., Gersonde, R., and Haug, G. H.: Subpolar Link to the Emergence of the Modern Equatorial Pacific Cold Tongue, *Science*, 328, 1550–1553, <https://doi.org/10.1126/science.1184480>, 2010.
- Martinez-Garcia, A., Rosell-Mele, A., Jaccard, S. L., Geibert, W., Sigman, D. M., and Haug, G. H.: Southern Ocean dust-climate coupling over the past four million years, *Nature*, 476, 312–315, 2011.
- Martinez-Boti, M. A., Foster, G. L., Chalk, T. B., Rohling, E. J., Sexton, P. F., Lunt, D. J., Pancost, R. D., Badger, M. P. S., and Schmidt, D. N.: Plio-Pleistocene climate sensitivity evaluated using high-resolution CO<sub>2</sub> records, *Nature*, 518, 49–54, <https://doi.org/10.1038/nature14145>, 2015.
- McClymont, E. L., Elmore, A. C., Kender, S., Leng, M. J., Greaves, M., and Elderfield, H.: Pliocene-Pleistocene evolution of sea surface and intermediate water temperatures from the Southwest Pacific, *Paleoceanography*, 31, 895–913, <https://doi.org/10.1002/2016PA002954>, 2016.
- McClymont, E. L., Haywood, A. M., and Rosell-Melé, A.: Towards a marine synthesis of late Pliocene climate variability, *Past Global Changes Magazine*, 25, 117, <https://doi.org/10.22498/pages.25.2.117>, 2017.
- McClymont, E. L., Ford, H. L., Ho, S. L., Alonso-Garcia, M., Bailey, I., Berke, M. A., Littler, K., Patterson, M. O., Petrick, B. F., Peterse, F., Ravelo, A. C., Risebrobakken, B., De Schepper, S., Swann, G. E. A., Thirumalai, K., Tierney, J. E., van der Weijst, C., and White, S.: Sea surface temperature anomalies for Pliocene interglacial KM5c (PlioVAR), *PANGAEA*, <https://doi.org/10.1594/PANGAEA.911847>, 2020.
- Medina-Elizalde, M. and Lea, D. W.: Late Pliocene equatorial Pacific, *Paleoceanography*, 25, PA2208, <https://doi.org/10.1029/2009pa001780>, 2010.
- Medina-Elizalde, M., Lea, D. W., and Fantle, M. S.: Implications of seawater Mg/Ca variability for Plio-Pleistocene tropical climate reconstruction, *Earth Planet. Sc. Lett.*, 269, 584–594, 2008.
- Mortyn, P. G. and Charles, C. D.: Planktonic foraminiferal depth habitat and δ<sup>18</sup>O calibrations: Plankton tow results from the Atlantic sector of the Southern Ocean, *Paleoceanography*, 18, 1037, <https://doi.org/10.1029/2001pa000637>, 2003.



- Müller, P. J., Kirst, G., Ruhland, G., Storch, I. V., and Rosell-Melé, A.: Calibration of the alkenone paleotemperature index  $U_{37}^k$  based on core-tops from the eastern South Atlantic and the global ocean (60° N–60° S), *Geochim. Cosmochim. Ac.*, 62, 1757–1772, 1998.
- O'Brien, C. L., Foster, G. L., Martinez-Boti, M. A., Abell, R., Rae, J. W. B., and Pancost, R. D.: High sea surface temperatures in tropical warm pools during the Pliocene, *Nat. Geosci.*, 7, 606–611, <https://doi.org/10.1038/ngeo2194>, 2014.
- Olsen, A., Key, R. M., van Heuven, S., Lauvset, S. K., Velo, A., Lin, X., Schirnick, C., Kozyr, A., Tanhua, T., Hoppema, M., Jutterström, S., Steinfeldt, R., Jeansson, E., Ishii, M., Pérez, F. F., and Suzuki, T.: The Global Ocean Data Analysis Project version 2 (GLODAPv2) – an internally consistent data product for the world ocean, *Earth Syst. Sci. Data*, 8, 297–323, <https://doi.org/10.5194/essd-8-297-2016>, 2016.
- Owens, M. J., Lockwood, M., Hawkins, E., Usoskin, I., Jones, G. S., Barnard, L., Schurer, A., and Fasullo, J.: The Maunder minimum and the Little Ice Age: an update from recent reconstructions and climate simulations, *J. Space Weather Spac.*, 7, A33, <https://doi.org/10.1051/swsc/2017034>, 2017.
- PAGES2k Consortium: A global multiproxy database for temperature reconstructions of the Common Era, *Scientific Data* 4, 170088, <https://doi.org/10.1038/sdata.2017.88>, 2017.
- Pelejero, C. and Calvo, E.: The upper end of the  $U_{37}^{K'}$  temperature calibration revisited, *Geochim. Geophys. Geosy.*, 4, 1014, 2003.
- Petrick, B., McClymont, E. L., Felder, S., Rueda, G., Leng, M. J., and Rosell-Melé, A.: Late Pliocene upwelling in the Southern Benguela region, *Palaeogeogr. Palaeoclimatol.*, 429, 62–71, <https://doi.org/10.1016/j.palaeo.2015.03.042>, 2015.
- Petrick, B., McClymont, E. L., Littler, K., Rosell-Melé, A., Clarkson, M. O., Maslin, M., Röhl, U., Shevenell, A. E., and Pancost, R. D.: Oceanographic and climatic evolution of the southeastern subtropical Atlantic over the last 3.5 Ma, *Earth Planet. Sc. Lett.*, 492, 12–21, <https://doi.org/10.1016/j.epsl.2018.03.054>, 2018.
- Philander, S. G. and Fedorov, A. V.: Role of tropics in changing the response to Milankovitch forcing some three million years ago, *Paleoceanography*, 18, 1045, 2003.
- Prahl, F. G. and S. G. Wakeham: Calibration of unsaturation patterns in long-chain ketone compositions for palaeotemperature assessment, *Nature* 320, 367–369, 1987).
- Prahl, F. G., Muehlhausen, L. A., and Zahnle, D. I.: Further evaluation of long-chain alkenones as indicators of paleoceanographic conditions, *Geochim. Cosmochim. Ac.*, 52, 2303–2310, 1988.
- Prescott, C. L., Haywood, A. M., Dolan, A. M., Hunter, S. J., Pope, J. O., and Pickering, S. J.: Assessing orbitally-forced interglacial climate variability during the mid-Pliocene Warm Period, *Earth Planet. Sc. Lett.*, 400, 261–271, <https://doi.org/10.1016/j.epsl.2014.05.030>, 2014.
- Rampen, S. W., Willmott, V., Kim, J.-H., Uliana, E., Mollenhauer, G., Schefuß, E., Sinninghe Damsté, J. S., and Schouten, S.: Long chain 1,13- and 1,15-diols as a potential proxy for palaeotemperature reconstruction, *Geochim. Cosmochim. Ac.*, 84, 204–216, <https://doi.org/10.1016/j.gca.2012.01.024>, 2012.
- Regenberg, M., Nürnberg, D., Steph, S., Groeneveld, J., Garbe-Schönberg, D., Tiedemann, R., and Dullo, W.-C.: Assessing the effect of dissolution on planktonic foraminiferal Mg/Ca ratios: Evidence from Caribbean core tops, *Geochim. Geophys. Geosy.*, 7, Q07P15, <https://doi.org/10.1029/2005GC001019>, 2006.
- Regenberg, M., Steph, S., Nürnberg, D., Tiedemann, R., and Garbe-Schönberg, D.: Calibrating Mg/Ca ratios of multiple planktonic foraminiferal species with  $\delta^{18}O$ -calcification temperatures: Paleothermometry for the upper water column, *Earth Planet. Sc. Lett.*, 278, 324–336, 2009.
- Rommerskirchen, F., Condon, T., Mollenhauer, G., Dupont, L., and Schefuß, E.: Miocene to Pliocene development of surface and subsurface temperatures in the Benguela Current system, *Paleoceanography*, 26, PA3216, <https://doi.org/10.1029/2010pa002074>, 2011.
- Rosell-Melé, A. and Prahl, F. G.: Seasonality of temperature estimates as inferred from sediment trap data, *Quaternary Sci. Rev.*, 72, 128–136, <https://doi.org/10.1016/j.quascirev.2013.04.017>, 2013.
- Rosell-Melé, A., Martínez-García, A., and McClymont, E. L.: Persistent warmth across the Benguela upwelling system during the Pliocene epoch, *Earth Planet. Sc. Lett.*, 386, 10–20, <https://doi.org/10.1016/j.epsl.2013.10.041>, 2014.
- Rosenthal, Y., Boyle, E. A., and Slowey, N.: Temperature control on the incorporation of magnesium, strontium, fluorine, and cadmium into benthic foraminiferal shells from Little Bahama Bank: Prospects for thermocline paleoceanography, *Geochim. Cosmochim. Ac.*, 61, 3633–3643, [https://doi.org/10.1016/S0016-7037\(97\)00181-6](https://doi.org/10.1016/S0016-7037(97)00181-6), 1997.
- Schiebel, R., Bijma, J., and Hemleben, C.: Population dynamics of the planktic foraminifer *Globigerina bulloides* from the eastern North Atlantic, *Deep Sea Research Part I: Oceanographic Research Papers*, 44, 1701–1713, [https://doi.org/10.1016/S0967-0637\(97\)00036-8](https://doi.org/10.1016/S0967-0637(97)00036-8), 1997.
- Schneider, B., Leduc, G., and Park, W.: Disentangling seasonal signals in Holocene climate trends by satellite-model-proxy integration, *Paleoceanography*, 25, PA4217, <https://doi.org/10.1029/2009pa001893>, 2010.
- Schouten, S., Hopmans, E. C., Schefuß, E., and Sinninghe Damsté, J. S.: Distributional variations in marine crenarchaeotal membrane lipids: A new tool for reconstructing ancient sea water temperatures?, *Earth Planet. Sc. Lett.*, 204, 265–274, 2002.
- Small, R. J., Curchitser, E., Hedstrom, K., Kauffman, B., and Large, W. G.: The Benguela Upwelling System: Quantifying the Sensitivity to Resolution and Coastal Wind Representation in a Global Climate Model, *J. Climate*, 28, 9409–9432, <https://doi.org/10.1175/jcli-d-15-0192.1>, 2015.
- Sonzogni, C., Bard, E., Rostek, F., Dollfus, D., Rosell-Melé, A., and Eglinton, G.: Temperature and salinity effects on alkenone ratios measured in surface sediments from the Indian Ocean, *Quaternary Res.*, 47, 344–355, 1997.
- Steph, S., Tiedemann, R., Groeneveld, J., Sturm, A., and Nürnberg, A. D.: Pliocene changes in tropical East Pacific Upper Ocean stratification: Response to tropical gateways?, *Proceedings of the Ocean Drilling Program. Scientific Results*, 202, 1–51, 2006.
- Steph, S., Tiedemann, R., Prange, M., Groeneveld, J., Schulz, M., Timmermann, A., Nürnberg, D., Rühlemann, C., Saukel, C., and Haug, G. H.: Early Pliocene increase in thermohaline overturning: A precondition for the development of the modern equatorial Pacific cold tongue, *Paleoceanography*, 25, PA2202, <https://doi.org/10.1029/2008pa001645>, 2010.
- Ternois, Y., Sicre, M. A., Boireau, A., Conte, M. H., and Eglinton, G.: Evaluation of long-chain alkenones as paleo-temperature in-

- dicators in the Mediterranean Sea, *Deep-Sea Res. Pt. I*, 44, 271–286, 1997.
- Tierney, J. E. and Tingley, M. P.: BAYSPLINE: A New Calibration for the Alkenone Paleothermometer, *Paleoceanography and Paleoclimatology*, 33, 281–301, <https://doi.org/10.1002/2017pa003201>, 2018.
- Tierney, J. E., Haywood, A. M., Feng, R., Bhattacharya, T., and Otto-Bliesner, B. L.: Pliocene Warmth Consistent With Greenhouse Gas Forcing, *Geophys. Res. Lett.*, 46, 9136–9144, <https://doi.org/10.1029/2019gl083802>, 2019a.
- Tierney, J. E., Malevich, S. B., Gray, W., Vetter, L., and Thirumalai, K.: Bayesian calibration of the Mg/Ca paleothermometer in planktic foraminifera, *Paleoceanography and Paleoclimatology*, 31, 2005–2030, <https://doi.org/10.1029/2019PA003744>, 2019b.
- Tripathi, A. K., Eagle, R. A., Thiagarajan, N., Gagnon, A. C., Bauch, H., Halloran, P. R., and Eiler, J. M.: <sup>13</sup>C–<sup>18</sup>O isotope signatures and ‘clumped isotope’ thermometry in foraminifera and coccoliths, *Geochim. Cosmochim. Ac.*, 74(20), 5697–5717, 2010.
- Wara, M. W., Ravelo, A. C., and Delaney, M. L.: Permanent El Nino-Like Conditions During the Pliocene Warm Period, *Science*, 309, 758–761, 2005.
- Zhang, Y. G., Pagani, M., and Liu, Z.: A 12-Million-Year Temperature History of the Tropical Pacific Ocean, *Science*, 344, 84–87, <https://doi.org/10.1126/science.1246172>, 2014.